THE ROSS SEA RESPONSE TO EVOLVING OCEAN-ICE INTERACTIONS IN A CHANGING CLIMATE

A Dissertation

by

CHRISTINA LEE WIEDERWOHL

Submitted to the Office of Graduate Studies of
Texas A&M University
in partial fulfillment of the requirements for the degree of

DOCTOR OF PHILOSOPHY

Approved by:

Chair of Committee,	Alejandro H. Orsi
Committee Members,	Achim Stoessel
	Mahlon C. Kennicutt
	Gerald North
Head of Department,	Piers Chapman

December 2012

Major Subject: Oceanography

ABSTRACT

Early 1990s to late 2000s freshening ($\Delta S \approx -0.001$–0.002) and warming ($\Delta\theta \approx$ 0.02°C–0.035°C) of bottom waters was detected in the southern Pacific Ocean, and Ross Sea source waters progressively freshened during the past four decades. This study investigates potential freshwater anomaly sources and quantifies their effect.

Glacial melt water inputs to the GCT increased by 1.3 km^3 per decade (1976–2007), more rapidly so after 2000 (6.8 km^3 per decade), freshening local Shelf Water by 0.0004 per decade. Lighter basal melt inputs to the LAT started in 1994 and also picked up after 2000 to 14.9 km^3 per decade, lowering the local Antarctic Surface Water salinity by -0.017 per decade. Upstream in the Amundsen Sea surface water freshened by -0.03 per decade (1994–2007) mostly (50%) from larger melt water inputs from the Pine Island (17.7 km^3 per decade) and Dotson (14.8 km^3 per decade) glaciers.

Two decades of steady (1978-2000) strengthening of sea ice productivity (200 km^3 per decade) within the Ross Sea Polynya suddenly reversed to weakening (-98.6 km^3 per decade) and resulted in Shelf Water freshening (-0.02 per decade) thereafter. To fully account for the observed variability in Ross Sea waters, the progressive (1992-2011) adjustment of the density field and induced advective contributions are estimated based on a simplified three-layer stratification. Eastern (western) inflow (outflow) of light surface (dense shelf) water increased by 28% (15%) to 1.11 Sv (1.01 Sv) by 2011; whereas a sluggish intermediate inflow (0.02 Sv) of Modified Circumpolar Deep Water

turned into outflow after 2007, thus contributing 0.09 Sv by 2011 to the ventilation of deep waters farther offshore.

The estimated evolution of overturning and advective salt fluxes in the Ross Sea yield overall freshening of water masses similar to those derived from observations. Volumetric mean salinities declined at -0.07 per decade for Antarctic Surface Water, -0.05 per decade for Modified Circumpolar Water, and -0.03 per decade for Shelf Water. Outflow intensification of Shelf Water mixtures is also consistent with bottom water property changes (freshening and warming) measured farther downstream in the southern Pacific Ocean.

DEDICATION

To Channing: May you one day find the mystery

and intrigue of science as exciting as I do

ACKNOWLEDGMENTS

A tremendous amount of gratitude goes to my committee chair, Dr. Alejandro H. Orsi. His excellent guidance, unwavering patience, tremendous encouragement, and financial support are what made this research possible. Thank you also to my committee members Dr. Achim Stoessel, Dr. Mahlon Kennicutt, and Dr. Gerald North for their valuable input and expertise throughout the course of this work. I would like to also acknowledge the National Science Foundation whose funding supported this research.

Thank you to the Department of Oceanography who provided numerous resources, which aided in the completion of this dissertation. A special thank you goes to Yong Sun Kim and Kelly Cole for their help in various capacities during the course of this work.

To my husband, Brian, I own an infinite amount of gratitude for his countless hours of love, support, and encouragement; and to my daughter, Channing, for making every day brighter and full of wonder.

NOMENCLATURE

AABW	Antarctic Bottom Water
AASW	Antarctic Surface Water
ACC	Antarctic Circumpolar Current
ACoC	Antarctic Coastal Current
ADW	Antarctic Deep Water
ALBW	Adelie Land Bottom Water
CDW	Circumpolar Deep Water
CLIVAR	Climate Variability and Predictability
Co11	Comiso et al. [2011]
GCT	Glomar Challenger Trough
HSSW	High Salinity Shelf Water
ISW	Ice Shelf Water
JG10	Jacobs and Giulivi [2010]
LAT	Little America Trough
LCDW	Lower Circumpolar Deep Water
LSSW	Low Salinity Shelf Water
MCDW	Modified Circumpolar Deep Water
MOC	Meridional Overturning Circulation
MSW	Modified Shelf Water
MWF	Melt Water Fraction

NADW	North Atlantic Deep Water
OW05	Orsi and Whitworth III [2005]
OW09	Orsi and Wiederwohl [2009]
PIG	Pine Island Glacier
RIS	Ross Ice Shelf
S06	Stover [2006]
SAM	Southern Annular Mode
SW	Shelf Water
TG	Thwaites Glacier
WOCE	World Ocean Circulation Experiment

TABLE OF CONTENTS

Page

LIST OF FIGURES

Page

Page

LIST OF TABLES

Page

CHAPTER I

INTRODUCTION

Background

It has long been recognized that the Southern Ocean interacts with the polar atmosphere and cryosphere year-round through active exchange of heat and freshwater over the Antarctic continental margins [*Deacon*, 1937; 1984; *Wust*, 1935]. Evolving atmospheric climate signals are quickly transferred to the polar regions through these interactions. Dense water masses formed at key locations in the Antarctic margins carry these signals away from their shallow sources via fast moving deep boundary currents to the abyssal layers of the world ocean (Figure 1.1).

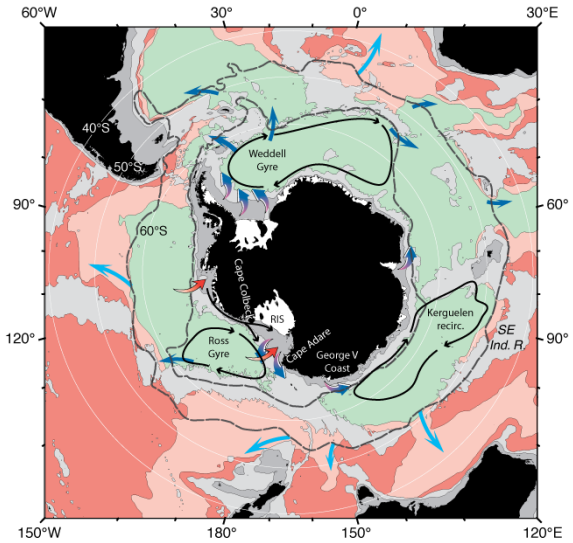

Figure 1.1. Schematic of the Southern Ocean circulation. Red (purple) arrows across the shelf break indicate inputs (outputs) of CDW (new AABW) to the shelf (deep ocean). Dark (light) blue arrows in the oceanic regime correspond to northward pathways of AABW (ACCbw). Bottom waters denser (lighter) than γ^n = 28.28 kg m^{-3} (γ^n = 28.20 kg m^{-3}) are shaded green (red); pink shaded areas have intermediate bottom densities. Grey dashed lines trace the mean locations of the Subantarctic Front and the Southern Boundary of the ACC. Water depths shallower than 3500 m (800 m) are shaded light (dark) grey. Continents are shown in black. Figure adapted from Orsi [2010].

The harsh and isolated nature of the Antarctic environment has made it difficult for oceanographers to measure along the various outflow paths of these dense waters. For many years the lack of adequate observations hindered a full assessment of the magnitude of change in the Southern Ocean's climate. Nonetheless, temperature and salinity characteristics of deep Southern Ocean waters have evolved during the past few decades with apparent significant trends [*Aoki et al.*, 2005a; *Aoki et al.*, 2005b; *Gille*, 2002; *Jacobs*, 2006; *Jacobs et al.*, 2002; *Johnson and Orsi*, 1997; *Johnson and Doney*, 2006; *Johnson et al.*, 2007; *Rintoul*, 2007; *Robertson et al.*, 2002; *Zenk and Morozov*, 2007]. Not well understood, however, is what drives the observed changes over the continental margins or what ramifications these signals have once engrained in new deep waters exported offshore, that feed the lower limb of the Meridional Overturning Circulation (MOC).

Stratification and Circulation of the Southern Pacific Ocean

North Atlantic Deep Water (NADW) enters the eastward-flowing Antarctic Circumpolar Current (ACC) from the South Atlantic as a deep (~2500 m) salty layer that progressively mixes with fresher surrounding waters above and below to produce the bulk of Circumpolar Deep Water (CDW) [*Worthington*, 1981]. Upon reaching Drake Passage the salinity maximum of CDW is ~0.10 fresher than at its source region in the Atlantic sector. On its poleward path toward the Antarctic continental margins, CDW shoals significantly across the ACC [*Callahan*, 1972; *Sievers and Nowlin*, 1984; *Sverdrup*, 1940; *Whitworth and Nowlin*, 1987], where, at the southern edge is identified as a thick intermediate layer of relatively warm, salty and oxygen-poor water. Only the

Lower portion of CDW (LCDW) is able to continue further south and flow within the colder sub-polar regime circulations [*Orsi et al.*, 1995].

In the Pacific sector a large cyclonic circulation, the Ross Gyre, draws in LCDW at its eastern limb, becoming the major source of heat and salt for regions farther to the west [*Locarnini*, 1994]. Upon reaching the continental slope of the Ross Sea, LCDW is often wedged between much colder waters above, Antarctic Surface Water (AASW), and below, Shelf Water (SW) [*Whitworth et al.*, 1998]. Onshore transport of LCDW is thought to be sporadic and occur only at specific locations likely dictated by the shelf topography [*Dinniman et al.*, 2003]. During the short transit across the shelf break, the warm and salty signals of LCDW are rapidly attenuated by diapycnal mixing with relatively fresh ($S < 34.4$) near-freezing AASW, resulting in what is commonly known as Modified Circumpolar Deep Water (MCDW) [*Newsom et al.*, 1965].

Because of air-sea-ice interactions, AASW shows a large seasonal range of potential temperatures (θ = -2.3°C to 2.0°C) and salinities ($S \approx 33.0$ to 34.4). While this is an extensive range, there is a clear distinction between AASW found over the oceanic versus shelf regimes. In the oceanic regime, this water extends from the sea surface to the shallow (~50 m to 100 m) base of the winter mixed layer, indicated by a subsurface temperature minimum in the summer [*Whitworth et al.*, 1998]. Relatively warm summer varieties of AASW are typically found along the southern continental shelf of the Ross Sea, where the pack ice opens up first each season [*Jacobs et al.*, 1970]. Here, the combined winter surface cooling of AASW and the shoaling of MCDW to near the sea surface, and the sustained sea-ice formation within two narrow coastal polynyas off

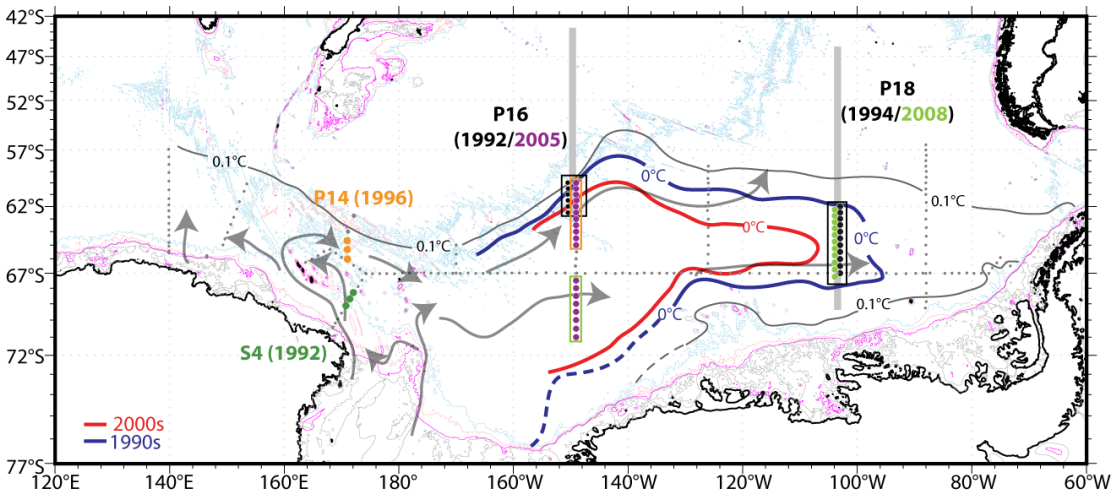

Figure 1.2: Inferred bottom circulation for the South Pacific. Bottom 0°C isotherm for the 1990s (2000s) is indicated by the thick blue (red) line. Bold colored dots show the location of stations used in Figure 2.4: a) black/purple (black/light green) dots enclosed by the black box along 150°W (103°W), b) purple (green) dots in green (black) box along 150°W (103°W), and c) purple dots in orange box along 150°W and orange (dark green) dots along 170°E. The thick meridional grey lines indicate the locations of the vertical sections shown in Figure 2.5. Thin grey dots are station location containing profiles with AABW (γ^n > 28.27 kg m^{-3}). Isobaths shown are the 500 (grey), 1000 (magenta), 2000 (light pink), and 3000-m (light blue).

Victoria Land (Terra Nova Bay Polynya) and the Ross Ice Shelf (Ross Ice Shelf Polynya; grey shade, Figure 1.2) contribute to the formation of a much saltier (S > 34.45) water mass than any AASW observed in the oceanic domain – the Shelf Water (SW) [*Locarnini*, 1994; *Smethie and Jacobs*, 2005]. Found only found over the continental shelf, this water acquired neutral densities greater than 28.27 kg m^{-3} [*Whitworth III et al.*, 1998] from buoyancy loss, and shows a relatively narrow range of near freezing potential temperatures (θ > -1.85°C) [*Orsi and Wiederwohl,* 2009; herein OW09] but a broad range of salinities, up to 35 [*Carmack*, 1977].

Shelf Water has been regionally classified into relatively salty and fresh types [*Jacobs et al.*, 1970] based on a sharp zonal salinity gradient near 175°W [*Locarnini*, 1994; *Orsi et al.*, 1999], even though both varieties are found in each region albeit with

the noticeable predominance indicated above. A volumetric analysis of SW salinities shows a relative θ-S void near S = 34.62 (Figure 1.3), thus this salinity value has been adopted to distinguish between low (LSSW) and high (HSSW) salinity varieties of SW in the Ross Sea [OW09].

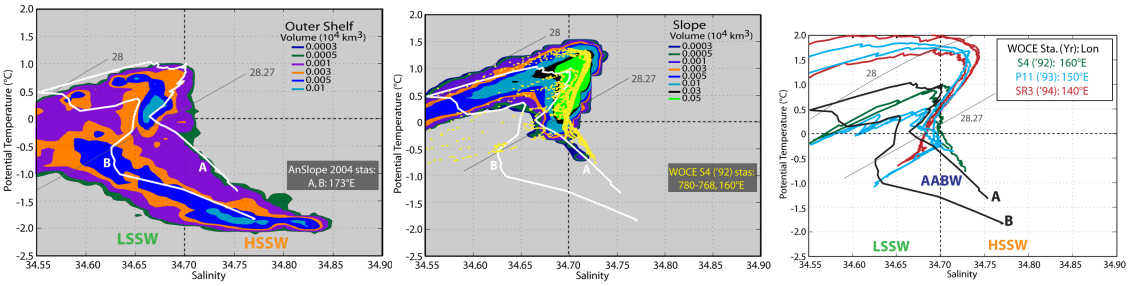

Figure 1.3: Volumetric θ-S census for the western Ross Sea shelf break. The a) outer shelf and b) slope regimes shown here are adapted from Orsi and Wiederwohl [2009]. White traces are selected 2004 AnSlope stations A (#31) and B (#93). b) Yellow dots show θ-S traces for S4 stations (#768-780). c) θ-S properties for selected stations from S4 (dark green); P11 (light blue) stations (#46, 56, 60, and 61); SR3 (red) stations (#64, 65, and 68); and AnSlope (black) are shown by thin traces. The locations of these station are shown in Figure 1.4.

The bulk of HSSW flows cyclonically within western troughs [*Budillon et al.*, 2002] and away from the production sites. Some HSSW flows under the 200-250 m deep Ross Ice Shelf (RIS), where it is further cooled from basal melt, and emerges around 180° as a relatively fresh (S ≈ 34.62) mid-depth plume commonly identified by potential temperatures below the sea surface freezing point (θ < -1.95°C) [OW09], thus named Ice Shelf Water (ISW; [*Budillon et al.*, 2002; *Carmack*, 1977; *Dinniman et al.*, 2003; *Lusquinos*, 1963; *Smethie and Jacobs*, 2005]). A less dense outflow of super-cooled water has also been found in the easternmost Ross Sea trough [*Locarnini*, 1994].

Intense vertical mixing of outflowing SW types with warmer MCDW above produces a relatively shallow water mass inshore of the sills of the Ross Sea troughs

named modified SW (MSW) [OW09]. An abundance (dark blue shade, Figure 1.3a) of this relatively fresh (S<34.7) and cold (-1.85°C < θ < -0.5°C) water is found above the regional HSSW. Some of this water near the shelf break sinks down slope to fill the abyssal layers of adjacent basins, where it is classically known as Antarctic Bottom Water (AABW) [*Foster and Carmack*, 1976; *Gill*, 1973; *Orsi and Wiederwohl*, 2009; *Orsi et al.*, 1999]. Forty percent of AABW is produced in the Indian-Pacific sector of the Antarctic continental margins [*Orsi et al.*, 1999], with outflows off the Adelie [*Gordon and Tchernia*, 1972; *Rintoul*, 1998] and George V coasts [*Carmack and Killworth*, 1978; *Foster*, 1995; *Jacobs*, 1989] and the Ross Sea [OW09]. Documented outflows of Ross Sea AABW are located near 173°E, 177°E, 175°W [*Jacobs et al.*, 1970], and 168°W [*Locarnini*, 1994]. In the past, the northwestern outflows have been on average the warmest (-0.6°C to -0.3°C) and saltiest (S > 34.75) around Antarctica, with an abyssal high-salinity (S > 34.70) signal extending over the northwest sector of the Pacific-Antarctic Basin [*Locarnini*, 1994]. In contrast, the AABW outflow found east of the Iselin Bank (168°W) is relatively cold (θ < 0°C) and fresh (S ≤ 34.70) [*Locarnini*, 1994; *Orsi et al.*, 1999].

The analysis of select hydrographic stations, including World Ocean Circulation Experiment (WOCE) and CLImate VARiability and predictability (CLIVAR) stations, allow for the construction of a schematic of the outflow paths shown in Figure 1.2. Low and high salinity varieties are clearly indicated off Cape Adare by the yellow θ-S scatter in Figure 1.3, corresponding to stations along the WOCE S4 line (black dots between 67°S and 71°S, Figure 1.4). The station traces overlap with the large volume of AABW

seen over the northwest slope regime in the Ross Sea climatology and with AnSlope station A (Figure 1.3b). Property vertical sections at S4 from the WOCE Southern Ocean Atlas [*Orsi and Whitworth III*, 2005b; herein OW2005] show a more detailed distribution of these two types of Ross Sea outflows. Both deep and bottom varieties are found along the slope as a westward-flowing relatively cold ($\theta < 0°C$) plume filling the bottom 1000 m of the water column (Plates 82 and 86 in OW05). Only the low salinity water turns cyclonically around the Balleny Islands, and back to the Pacific-Antarctic Basin. Properties along P14 (Plates 82 and 86 in OW05) show this eastward flowing water hugging the southern flank of the Pacific-Antarctic Ridge within a ~500 m thick bottom layer with relatively low salinities (~34.695) and temperatures ($\theta < 0°C$). This Ridge effectively blocks the northern extent of AABW outflows from the Ross Sea, whereas they continue unobstructed towards Drake Passage underneath the ACC, and into the Australian-Antarctic Basin along the continental rise (grey arrows, Figure 1.2). Thus Ross Sea sources of AABW effectively freshen and ventilate both the Pacific and Indian sectors of the Southern Ocean [*Orsi et al.*, 1999].

Also contributing to the deep ocean ventilation is a slightly lighter SW mixture (Figure 1.3) exported from the Ross Sea at levels above AABW [OW09]. This upper portion of MSW flows out of the Ross Sea along isopycnals as an export of low salinity AABW and MCDW that is less restricted by the sills, and therefore also more likely to transfer atmospheric and upper water anomalies rapidly to the deep ocean.

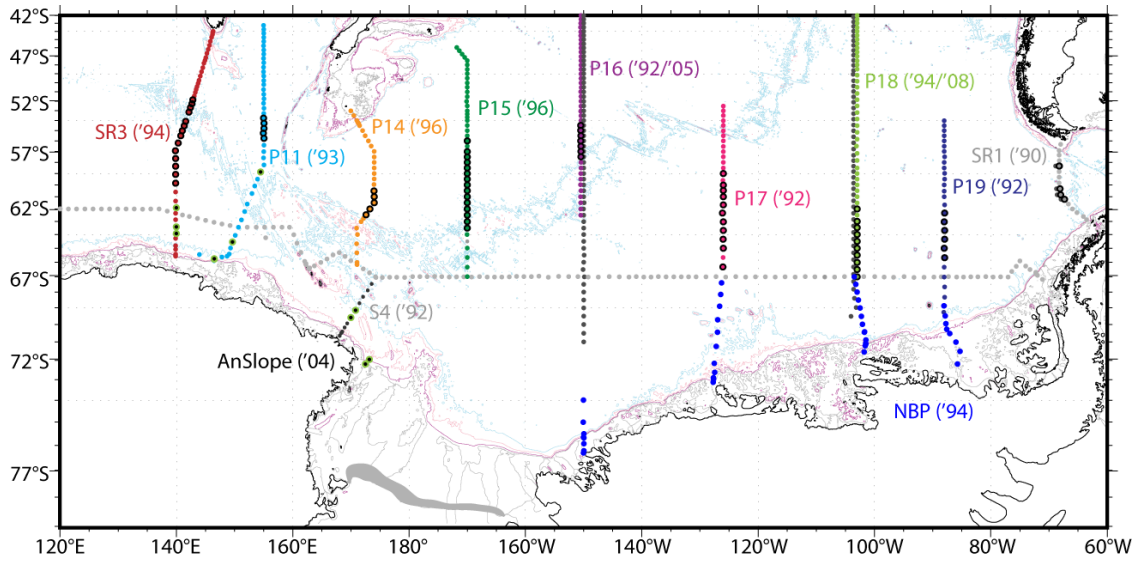

Figure 1.4: Location of South Pacific stations. WOCE/CLIVAR data (colored dots) displayed in Figures 2.2 and 2.3 are indicated by dots with a thick black outline. NBP9402 stations (blue dots) used to connect the WOCE/CLIVAR transects to the coast are shown. Black dots with a thick green outline are the location of stations used in Figure 1.3. The mean location of the RIS Polynya from Arrigo and van Dijken [2003] is shown by the grey shaded area along the RIS.

Evidence of Decadal Variability in Antarctic Water Properties

Table 1.1 lists more details on the ongoing deep-water changes discussed next. By comparison to the Australian-Antarctic Basin, little has been reported on deep-water variability in the South Pacific Ocean [*Aoki et al.*, 2005a; *Aoki et al.*, 2005b; *Jacobs*, 2006; *Rintoul*, 2007]. Surface waters have also progressively freshened in the Amundsen Sea Embayment from 1994 to 2000 [*Jacobs*, 2006], a large and well-known area of increasing basal melt rates and ice shelf erosion triggered by inshore fluxes of warmer (1994 – 2009) CDW [*Jacobs et al.*, 2011] from the oceanic regime [*Jacobs et al.*, 1996; *Jacobs et al.*, 2011; *Rignot et al.*, 2008]. This signal is thought to be transferred to the Ross Sea via the Antarctic Coastal Current (ACoC) [*Jacobs*, 2006; *Jacobs et al.*, 2002]. Remnants of this signal are still apparent in the AASW found in front of the RIS, where

Table 1.1. List of reported decadal temperature and salinity changes in the Indian and Pacific sectors of the Southern Ocean.

Reference	Region	Water mass	Δt (yrs)	ΔS	Δθ (°C)
Jacobs (2006)	Amundsen	AASW	1994-2000	-0.025	--
Jacobs and Giulivi (2010)	Amundsen	CDW	1994 – 2009	--	0.1-0.2
Jacobs and Giulivi (2010)	RIS	AASW	1967-2007	-0.32	--
Jacobs et al. (2002)	Ross Gyre	CDW	1960-2000	--	+0.26
Stover (2006)	180°	CDW	1964-2004	0.03	0.3
Jacobs and Giulivi (2010)	RIS	MCDW	1976-2007	-0.12	-0.5
Jacobs and Giulivi (1998)	RIS (173-174°W)	MCDW	1967-1994	-0.06	-0.4
Stover (2006)	180°	MCDW	1959-2004	-0.11	-1.25
Williams et al. (2006)	Drake Passage	CDW	1926-2004	0	0
Jacobs et al. (2002)	Ross Is.	SW	1963-2000	-0.111	--
Jacobs and Giulivi (2010)	Ross Is.	SW	1958-2008	-0.15	0.01
Jacobs et al. (2002)	RIS	SW	1960-2000	-0.13	--
Jacobs and Giulivi (2010)	Cape Adare	AABW	1959-2008	-0.04	0
Rintoul (2007)	170°E	AABW	1967-1996	~ -0.015	-0.2
Aoki et al. (2005)	140°E	AABW (γ^n = 28.35)	1994-2002	-0.03	--
Jacobs and Giulivi (2010)	George V Coast	AABW	1950-2005	-0.066	--
Rintoul (2007)	115°E, 61°S–63.3°S	AABW	1995-2005 1970-2005	-0.018 -0.02	-0.09 --
Purkey and Johnson (2010)	SW Pac. Basin	AABW	1992-2008	--	0.03
Ozaki et al. (2009)	North Ross Sea	AABW	1974-2004 1969-2004	-0.02 -0.018	0.074 0.193

a long-term (1967-2007) freshening has been reported [*Jacobs and Giulivi,* 2010; herein JG10].

CDW within the southern limb of the Ross Gyre shows evidence of change during the past four decades (1960-2000): a warmed and shoaled temperature maximum (Table 1.1) [*Jacobs et al.*, 2002] indicative of a continued strengthening of that subpolar cyclonic circulation. Just offshore of the shelf break and west of the Iselin Bank, CDW warming and increasing salinity trends are found during roughly the same period [*Stover,* 2006; herein S06]. The opposite changes are apparent once this water progresses onto the shelf: inflowing MCDW in the western Ross Sea has cooled and freshened

during 1959-2004 [S06]. A similar shorter term freshening and cooling trend (1976-2007) is found for MCDW reaching the front of the RIS [JG10], consistent with earlier reports for 1967-1994 [*Jacobs and Giulivi,* 1998]. The temperature decrease is not a steady decline, with the largest cooling between the mid 1980s and 1994 [JG10]. In contrast, core properties of LCDW in Drake Passage have remained fairly constant since 1926 [*Williams et al.*, 2006]. It is speculated that this pattern is consistent throughout the South Pacific Ocean, based on the apparent lack of change in CDW properties south of Australia.

Near Ross Island, the salinity of the densest SW had decreased significantly (Table 1.1) from 1967 – 2002 [*Hellmer and Jacobs*, 1994; *Jacobs et al.*, 2002], a freshening trend further supported with an expanded time series (1950 – 2005) [JG10]. In long zonal repeat transects in front of the RIS, HSSW saltier than 34.9 was found in the 1960s is no longer present by 1976 [*Jacobs et al.*, 2002], since it freshened at a rate similar to that observed near Ross Island. Similarly, volumes of SW saltier than 34.8 have been drastically reduced from 1967 to 1994 [*Jacobs and Giulivi*, 1998].

The above-mentioned changes in Ross Sea source water masses must eventually have an impact on the properties of new bottom waters exported near the shelf break. Freshening of Adelie Land BW (ALBW) is already observed off the George V Coast from 1950 – 2005 (Table 1.1), where outflows of even less saline types of AABW are well documented [*Rintoul*, 2007]. South of the Polar Front in the Australian-Antarctic Basin, *Aoki et al.* [2005b] report freshening of ALBW during 1994 - 2002 and speculate the trend extends back to the 1960s. Further to the west along the continental rise

(~115°E) within the Australian-Antarctic Basin, colder and fresher ALBW (1995 – 2005) flows cyclonically within a deep boundary current system. Along the southern flank of the Southeast Indian Ridge Rintoul [2007] reports an even longer-term (1970-2005) freshening and cooling trend.

While JG10 attributed these changes to the salinity decrease in Ross Sea HSSW, inspection of selected stations within the Australian-Antarctic Basin (Figure 1.3c) reveals AABW with origins in other marginal areas. The θ-S traces below the CDW temperature maximum from P11 (blue) and SR3 (red) stations show AABW with contributions of much less saline local sources than those seen in the Ross Sea [*Gordon and Tchernia*, 1972; *Rintoul*, 1998]. Therefore both low and high salinity types of AABW are exported to the Australian-Antarctic Basin, whose abyssal layer is replenished by even fresher waters sinking downslope from local sources.

A significant freshening in the salinity of AABW exported from the northwest Ross Sea has been reported off Cape Adare from 1959 to 2008 (Table 1.1) [JG10]. A similar salinity decrease, in addition to warming, was found between 1969 and 2004 in the bottom layer just south of the Pacific-Antarctic Ridge [*Ozaki et al.*, 2009]. Comparison of primarily WOCE (1990s) and CLIVAR lines (2000s) indicate abyssal warming, with more prominent signals closer to the AABW southern sources [*Johnson et al.*, 2007]. *Purkey and Johnson* [2010] also estimated a warming trend in AABW (Table 1.1) below 3500 m for the entire Southern Pacific Basin.

Objectives

Inconsistencies and poorly known links between deep-water characteristics variability at the source continental margins, i.e. the Ross and Amundsen seas, warrant the detailed assessment of ongoing ocean climate changes in that region. Comparison of recent hydrographic data with the highest quality data sets from the 1990s - 2000s will not only allow us to determine the regional property distributions and circulation of the deep Pacific sector of the Southern Ocean, but they will also quantify decadal temperature and salinity signals in context, while also investigating their causes and impact on the MOC.

Shelf source regions will be investigated for any ongoing changes of glacial melt water inputs and sea ice production. For the first time, long-term trends of glacial melt water inputs from the RIS will be quantified, in combination with a revised sea-ice production rates. The effects of their associated freshwater anomalies on the local water masses will be evaluated in the following Chapters, as well as the evolution of volume transport of imported surface waters along the ACoC and of exported new deep and bottom waters out of the westernmost shelf troughs. Thus this study will analyze how local freshwater anomalies alter the production and sinking of new deep and bottom waters within the Ross Sea, and therefore also the lower limb of global thermohaline circulation.

CHAPTER II

OBSERVED DEEP SOUTH PACIFIC CHANGES

Available Data

This study uses the latest update of the Southern Ocean Database (SODB) maintained at TAMU [http://woceatlas.tamu.edu]. It consists of profile data from all available CTD and bottle casts occupied south of 25°S since 1906. We have recently conducted an extensive search of high-quality data available at the most reliable data centers around the globe to find potentially key missing hydrography, as well as more recent data sets collected in the past few years. All data have been individually quality controlled and erroneous data points have been flagged.

WOCE high-resolution full water column profiles of a suite of physical and chemical parameters were measured along a series of transects that crisscrossed the South Pacific Ocean between 1990 and 1996 with unprecedented spatial resolution (Figure 1.4). The shelf extensions of the easternmost WOCE lines were accomplished during a separate cruise on the Nathaniel B. Palmer in 1994 (blue dots, Figure 1.4). Only two of these meridional WOCE lines have been repeated in the past decade, during the CLIVAR Repeat Hydrography program: P16 in 2005 (purple dots; Figure 1.4) and P18 in 2008 (light green dots). CTD data from WOCE and CLIVAR are believed to have an accuracy of 0.003 for salinity and 0.002°C for temperature. Thus, their comparison is key to detect potential decadal variability in water mass properties, like

those already reported in the South Indian Ocean [*Aoki et al.*, 2005a; *Aoki et al.*, 2005b; *Johnson et al.*, 2008; *Rintoul*, 2007], and to estimate the spatial extent of these signals.

Standard Salinity Batch Corrections

Abyssal waters are effectively isolated from the sea surface processes that imprinted their thermohaline characteristics. Considering that WOCE measurements were made within a relatively short period of time, minimal differences in deep property values are expected at the intersection of WOCE transects. However, systematic comparison of crossover CTD stations from different cruises have shown systematic offsets in deep salinity values due to batch-to-batch differences in the Standard Seawater commonly used to calibrate CTD salinities [*Johnson et al.*, 2001; *Kawano et al.*, 2006]. To reduce these offsets, standard seawater batch corrections [*Kawano et al.*, 2006] were applied to all WOCE and CLIVAR CTD data as listed in Table 2.1. CTD salinities with and without these batch corrections from stations nearest to each crossover location (Figure 2.1) were inspected within a deep well-mixed layer (28.10 kg $m^{-3} < \gamma^n < 28.25$ kg m^{-3}) well below the NADW salinity maximum that shows minimum scatter.

Batch corrections narrowed most of the deep salinity gaps to differences below the accuracy of the instrument (Figure 2.1). Of the cruises analyzed, two appear to be too salty. Corrected data at the P18/S4 intersection show a salinity shift of ~0.003, which seems unrealistically too large within the minimum-variance layer. Farther to the north, the P18/P17e crossing more closely aligns when using the uncorrected P18 data. The same observation applies farther upstream in the ACC, at the WOCE P14/S4 and P15/S4 crossings.

Table 2.1. List of all standard seawater batch corrections applied to CTD salinities of WOCE and CLIVAR lines

WOCE/CLIVAR line	IAPSO Batch	Batch Correction
SR3	P-123	+0.0007
P11	P-121	+0.004
P14	P-114	+0.002
P15	P-114	+0.002
P16	P-120	-0.0009
P16 repeat	P-144	-0.0005
P17	P-120	-0.0009
P18	P-114	+0.002
P18 repeat	P-147	-0.0005
P19	P-120	-0.0009
SR1	P-120	-0.0009
S4	P-108	+0.0017

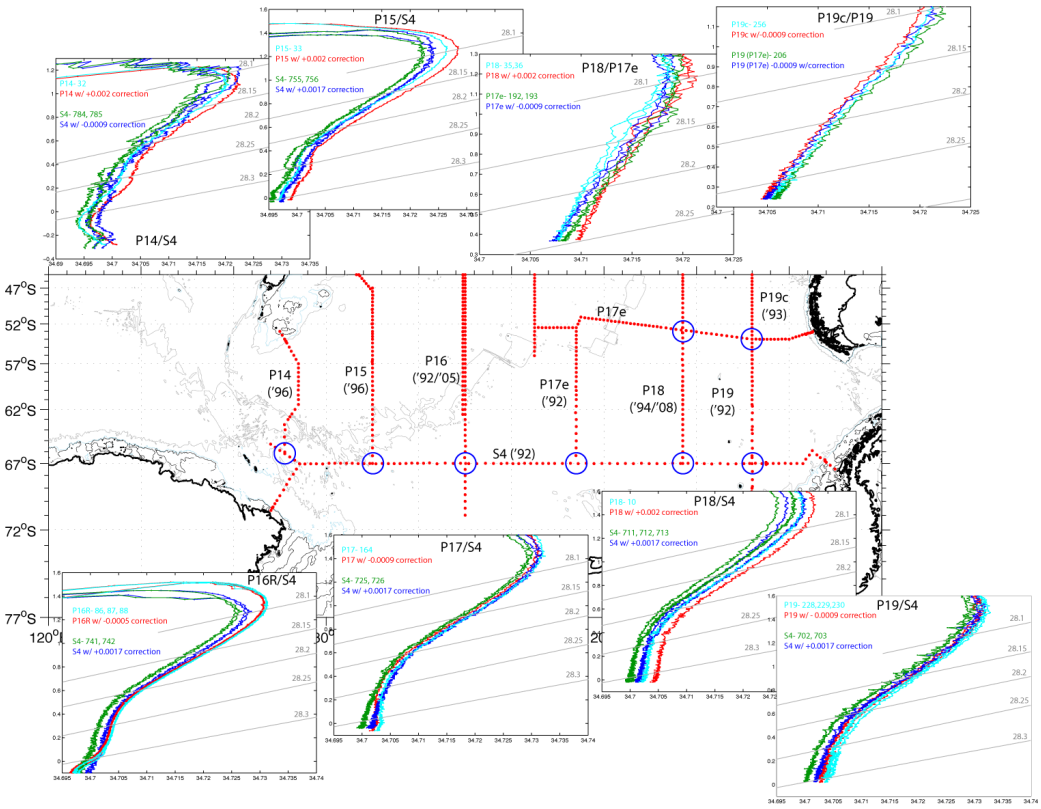

Figure 2.1: WOCE/CLIVAR cross over locations and their associated potential temperature versus salinity plots before and after batch correction. Cyan and green (red and blue) traces are before (after) batch corrections. Station numbers used for each cruise and the associated batch correction value are listed within each θ-S plot.

Both P14/P15 and P18 cruises used the same IAPSO standard seawater batch (P-114) and were all lead by the Pacific Marine Environmental Laboratory (PMEL). Thus we postulate that the discrepancies in these batch corrected salinities could result from either 1) the batch correction for P-114 given in Kawano et al. [2006] being incorrect or used "as needed"; or 2) differences in CTD data processing methods between PMEL and various other institutions, e.g. Scripps Institute of Oceanography.

Batch corrections are determined under controlled laboratory experiments, thus the likelihood that only the P-114 batch was incorrect seems small. While SeaBird Electronics provides suggested instructions on processing CTD data, there is no one common method accepted throughout the oceanographic community and, surprisingly, the CLIVAR community. Utilizing its own slightly different protocol, the PMEL processed data results in higher salinities. To avoid any unforeseen biases, batch corrections were applied to all data, and the effects of the "saltier" corrected PMEL data are inspected in relationship to the known circulation in the South Pacific.

Empirical Salinity Adjustments

To confirm the regional mixing pattern of CDW within the core of the ACC, θ-S traces of the deep salinity maximum layer (28.05 kg $m^{-3} < \gamma^n <$ 28.10 kg m^{-3}; Figure 2.2) from WOCE stations (black outlined circles, Figure 1.4) are inspected, e.g. the most "pure" un-ventilated salinity maximum derived from NADW at each meridional line. Only after batch corrections are applied, with two exceptions discussed below, is the expected progressive salinity decrease of from south of Australia (SR3; S = 34.75) to

Drake Passage (SR1; Figure 1.4) due to mixing with the fresher waters above and below along the flow path indicated.

An opposite regional mixing pattern is observed in the bottom layer ($\gamma^n > 28.20$ kg m^{-3}). The average θ-S traces and 1-std envelopes (Figure 2.3) were calculated for each group of ACC stations along the same WOCE line. Cold AABW gains salinity as it flows eastward away from the source regions and progressively mixes with the saltier CDW above. Bottom waters found at SR3 are the freshest (S<34.7) in the area and slowly gain salt toward Drake Passage where they are near S = 34.71. These opposite regional mixing patterns produce a unique "hour-glass" arrangement in the θ-S relationship of deep and bottom waters of the South Pacific Ocean. A thin mid-depth layer with uniform characteristics prevails in this sector of the Southern Ocean as indicated by the minimum θ-S scatter near θ = 0.6°C, S = 34.71 in the western sections (SR3 to P15) and near θ = 0.8°C, S = 34.715 in the eastern sections (P16 to P19; Figure 2.3b). The division of two different minima is likely due to the location of the "core" ACC stations with respect to the Pacific-Antarctic Ridge. While data from most WOCE lines agree well with the zonal mixing pattern described above, there are, however, slight discrepancies between two of the main sections.

The deep θ-S traces (Figure 2.3a) for the P11 (blue shade) and P18 (green shade) lines show bottom layer as well as salinity maximum characteristics (Figure 2.2a) that are much saltier than at the lines immediately downstream (eastward). We attribute these unrealistic salinity offsets throughout the water column to unregulated processing techniques used at different institutions. Therefore, to force agreement with the

regionally consistent deep-water envelopes shown in Figure 2.3b, the P11 and P18 salinity profiles were arbitrarily shifted by ad-hoc salinity corrections of -0.0065 and -0.0017 respectively. We also note that the same SeaBird CTD system was used both P18 occupations, thus the same salinity correction was applied to the CLIVAR P18 data.

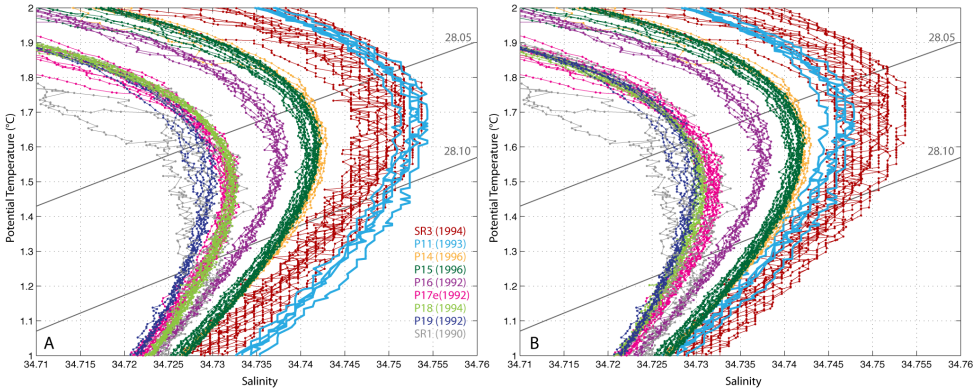

Figure 2.2: Potential temperature versus salinity for the deep salinity maximum. Color traces of stations a) before and b) after ad hoc adjustments correspond to individual WOCE lines whose locations are shown in Figure 1.4. The 28.05 kg m^{-3} and 28.10 kg m^{-3} neutral density lines are shown in grey.

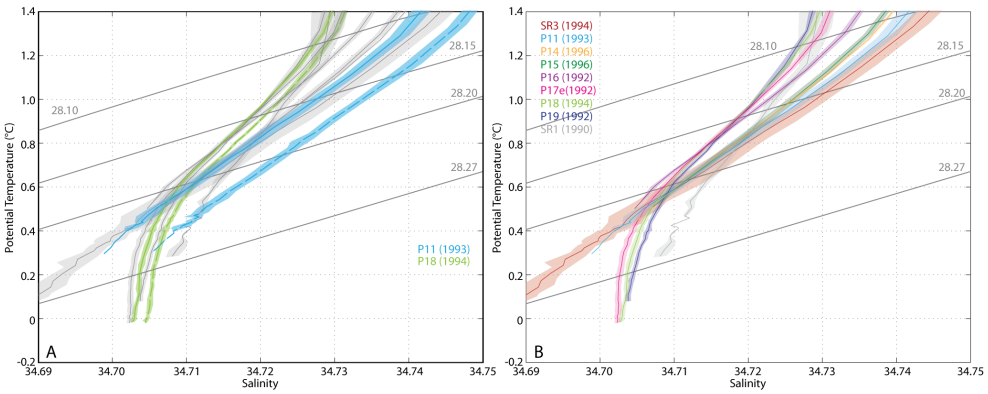

Figure 2.3: Mean one-standard deviation θ-S envelopes for select ACC stations from meridional WOCE lines. a) Envelopes for P11 (light blue) and P18 (light green) before (dashed line) and after (solid line) ad-hoc salinity corrections are shown with other WOCE line envelopes in light grey shades. b) Envelopes for all selected WOCE stations after all batch and ad-hoc salinity correction are applied. Colors correspond to individual WOCE lines shown in Figure 1.4. Grey lines are selected neutral density surfaces.

Incipient Evidence of Decadal Variability

While the spatial coverage of WOCE hydrographic data in the South Pacific sector of the Southern Ocean gives us a good snapshot of the regional circulation and water mass distribution, comparison of WOCE and CLIVAR repeat stations along the P16 and P18 lines (Figure 1.2) reveals significant changes in AABW properties (Figure 2.4). Below the relatively old mid-depth salinity maximum layer, warming and freshening of bottom waters denser than 28.27 kg m^{-3} are indicated along P16 by the clear divergence of purple scatter. Mean 1-std envelopes (not shown) constructed using data from all P16 stations that contain AABW ($\gamma^n > 28.27$ kg m^{-3}) show that properties just south of the Ridge have on average warmed by 0.035°C and freshened by ~0.001 over ~14 years. The same pattern of change is found farther downstream using profiles along P18 (Figure 1.2). The 1994 stations (black dots, Figure 2.4) show bottom waters colder than 0°C and saltier than 34.703. During the reoccupation of this line in 2008, stations within the same latitude band reveal the lack of any AABW colder than 0°C (green dots). One-std envelopes of AABW property differences show that the bottom 400 m appear to be fresher and warmer with an average salinity decrease of ~0.002 and temperature increase of 0.02°C over 14 years.

The re-occupation of the P16 line extended much farther to the south (71°S) in 2005 than in 1992 (62°S). The θ-S properties of stations located south of the Ridge show at least three different families between -0.1°C and 0.2°C (Figure 2.4b) separated by two θ-S voids. These voids are likely originating from interactions with fracture zones along the northern limb of the Ross Gyre. The coldest ($0°C < \theta < 0.25°C$) and saltiest of these

families (purple dots, Figure 2.4b), when compared to the CLIVAR P18 stations (green dots) farther downstream, show almost identical θ-S characteristics in waters denser than γ^n = 28.27 kg m^{-3} – indicating that these waters are connected by streamlines. The warmer θ-S void (0.3°C -0.6°C) is likely due to waters of interacting with the Ridge farther upstream.

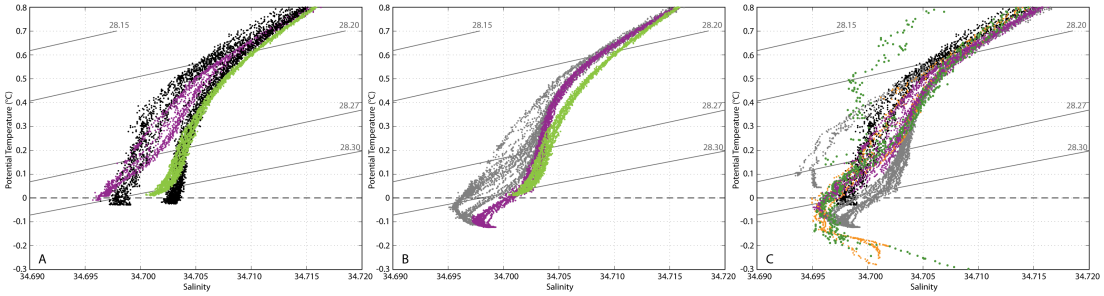

Figure 2.4: Potential temperature versus salinity profiles for selected WOCE/CLIVAR stations. Stations along a) WOCE (CLIVAR) P16 and P18 are indicated by black (colored) dots, b) CLIVAR P16 (P18) by grey and purple (green) dots, and c) WOCE P14 (S4P) stations by orange (dark green) dots. The location of these stations is shown in Figure 1.2.

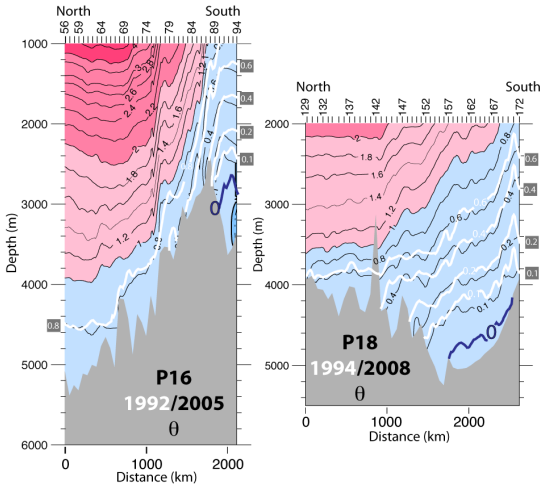

Figure 2.5: Vertical sections of deep potential temperature distribution for CLIVAR P16 and P18. Isotherms from corresponding WOCE (1990s) are shown by the white traces with the 0°C isotherm in blue. The location of these sections is shown in Figure 1.2.

The warmest and freshest of these CLIVAR P16 families (purple dots, Figure 2.4c) shows deep θ-S properties identical to those found on the WOCE P14 line south of the Pacific-Antarctic Ridge (orange dots, Figure 1.2; 2.4). P14 stations located to the north of the Ridge (grey dots) display more "ACC-like" properties above 0.2°C, whereas those to the south have properties that can be traced back to sources at the northwest Ross Sea slope. Stations found along the slope just off of Cape Adare (dark green dots, Figure 1.2) collected in 1992 show cold (θ < -0.3°C), salty (S>34.71) HSSW near the bottom, overlain by fresher (S < 34.7) LSSW. Here, relatively cold (θ < 0°C) non-bottom water has the same θ-S properties found north of the Balleny Islands along P14 (Figure 2.4c) and is eventually found within the bottom layer at 150°W, just south of the Ridge (purple dots).

Inspection of the deep water column along the P16 and P18 lines (Figure 2.5) reveals a reduction in the "volume" (area) of AABW colder than 0°C. In 2005, this once thick (1000 m) layer of relatively cold water is only detected in the southern most station and has mostly been replaced with relatively warmer bottom water varieties with θ = ~0.1°C. However, the vertical location of the 0.1°C isotherm along P16 in 1992 did not change significantly in 2005. P18 shows a very similar pattern: bottom waters colder than 0°C (~300-m thick) found throughout the southernmost (south of 61°S) 1994 stations were not measured in 2008 and slightly warmer waters (~0.1°C) remained unchanged. This indicates that the "volume" of relatively fresh AABW with ~0.1°C must have increased to replace the void induced by the vanishing saltier and colder (< 0°C) bottom water during WOCE. In addition to the reduction in thickness, a clear

retreat in the aerial extent of the bottom 0°C isotherm toward the Ross Sea sources is inferred during the past 14 years, as indicated by the bottom potential temperature map shown in Figure 1.2 constructed using all WOCE and CLIVAR data.

The lack of temperature differences in the warmer mid-depth waters (Figure 2.5), points to a southern source of change. Slope stations (Figure 2.6) along the main outflow of new Ross Sea bottom waters show a progressive freshening (-0.032 per decade) of deep and bottom water since 1967 (blue traces). Tracing these θ-S tails to the surface freezing point shows the evolution of the parent water mass, SW. By 2011, the high salinity ($S > 34.7$) SW end member is no longer a main ingredient of this new outflow, indicating that in recent years the relatively low-salinity and well-ventilated types of MCDW and AABW exported at the Antarctic Slope Front play progressively greater roles in replenishing the deep and bottom layers of the Pacific sector of the Southern Ocean.

This study attempts to explain these observed anomalies in oceanic deep-water characteristics in relation to evolving processes and air-sea-ice interactions within the Ross Sea shelf. In the next chapters the potential sources of freshwater and heat anomalies within the Ross Sea shelf are investigated.

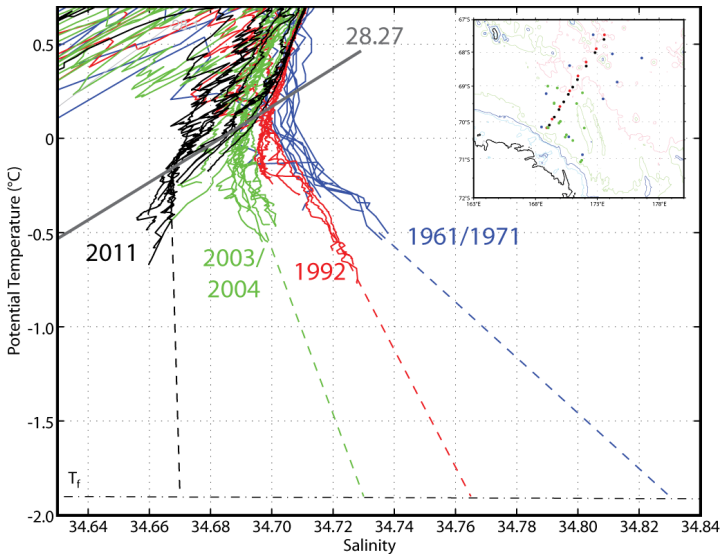

Figure 2.6: Potential temperature versus salinity for AABW along the slope near Cape Adare. Selected stations from 1967/1971 (blue), 1992 (red), 2003/2004 (green), and 2011 (black) are shown. Vertical dashed lines are extrapolated from the θ-S curves to the freezing point (horizontal dash-dot line) to show the approximate salinity of its parent Shelf Water. Grey traces are selected isopycnal surfaces. The inset map shows the location of these stations. Blue and red stations were shown in Rintoul [2007] and green stations were shown in Jacobs and Giulivi [2010].

CHAPTER III

GLACIAL MELT WATER CONTRIBUTIONS TO THE ROSS SEA

Introduction

The significant freshening of Ross Sea water masses observed during the past few decades is widely speculated [*Jacobs*, 2006; *Jacobs and Giulivi*, 2010] to be the result of massive freshwater anomalies from glacial melt water inputs over marginal regions farther upstream, e.g. in the Amundsen Sea. The entire Antarctic ice sheet contributes annually to the Southern Ocean about 138 Gt (1 Gt $=10^{15}$ kg) of freshwater through calving and melt water discharge [*Jacobs et al.*, 1992; *Rignot et al.*, 2008]. The greatest losses are at the Pine Island (PIG) and Thwaites (TG) glaciers, which have more than doubled from 41 Gt per year (a^{-1}) in 1996 to 90 Gt a^{-1} in 2006 [*Rignot et al.*, 2008]. Farther to the west, the Getz Ice Shelf was reduced by 19 Gt a^{-1} in 2000 [*Rignot et al.*, 2008]. In contrast, the 2000 glacial inputs to the RIS outweighed losses by only 13 Gt a^{-1} not only because it is far more distant to the oceanic heat source, but also due to a much larger buttressing than for the PIG and TG.

One of the largest threats to the stability of floating ice shelves is the availability and cross-shelf access of relatively warm oceanic waters. Heat content of seawater that flows into an ice shelf cavity has the potential to melt its underside, in direct proportion to the temperature anomaly with respect to the in-situ freezing point of seawater, which is particularly large at deep grounding lines. This chapter quantifies glacial melt water

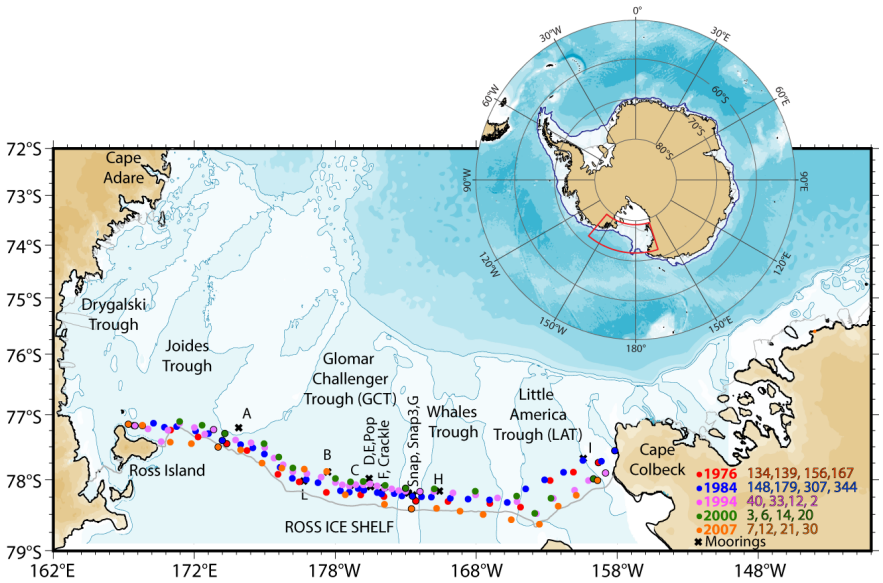

Figure 3.1: Basemap of RIS sections. CTD station locations (dots) are colored by year whereas the black x indicates a historical mooring location. Selected stations with a black outline are listed from west to east to the right of the legend.

sources in the Pacific sector of the Southern Ocean and investigates their effect on the local water mass stratification.

Hydrographic Data

Bottle data from six cruises between 1936 and 1967 were used to inspect any historical occurrences of ISW in the Glomar Challenger Trough (GCT) and Little America Trough (LAT). To date, only five synoptic sections since 1976 span the entire length of the RIS front from Ross Island to Cape Colbeck with full water column CTD profiles (Table 3.1; colored dots, Figure 3.1). The mean station spacing from these five years is fairly consistent, with the highest resolution (7.2 km) in 1984 and the lowest (13.3 km) in 1976. All cruises reflect summer conditions, thus any property differences are likely not due to a seasonal bias.

Table 3.1. List of cruises used for the RIS melt water estimates. The location of these stations is shown in Figure 3.1.

Year	Cruise	Dates	No. of stations	Mean station spacing (km)
1976	Northwind	21 Dec. – 24 Dec.	17	13.3
1984	Polar Sea	22 Jan. – 28 Jan.	35	7.2
1994	Polar Sea	5 Feb. – 10 Feb.	38	8.2
2000	NBP0001	15 Feb. – 18 Feb.	18	13
2007	NBP0702	8 Feb. – 11 Feb.	21	12.1

Table 3.2. Meta information and mean properties for historical moorings located in front of the RIS.

Mooring	Latitude	Longitude	Instrument Depth (m)	Water Depth (m)	Dates	Mean U Velocity (cm s^{-1})	Mean V Velocity (cm s^{-1})	Mean PTM (°C)
A	-77.207	175.155	175	685	23 Jan 84 - 21 Feb 84	---	---	-1.925
			350		23 Jan 84 - 21 Dec 84	-6.191	2.778	-2.063
B	-77.882	-178.533	340	700	24 Jan 84 - 06 Feb 85	4.051	0.748	-1.925
			425		24 Jan 84 - 19 Oct 84	5.186	2.826	-2.063
			650		24 Jan 84 - 06 Feb 85	2.526	2.366	-1.924
C	-78.078	-176.658	220	595	24 Jan 84 - 24 Mar 84	-2.324	-2.871	-1.127
			425		24 Jan 84 - 30 Nov 84	1.384	3.369	-1.735
D	-78.098	-175.503	125	558	25 Jan 84 - 04 Feb 85	-5.453	0.691	-1.685
			225		25 Jan 84 - 04 Feb 85	-4.720	1.245	-1.477
			300		25 Jan 84 - 04 Feb 85	-4.611	0.019	-1.500
E	-77.978	-175.597	210	585	25 Jan 84 - 05 Feb 85	-1.782	1.095	-1.532
			285		25 Jan 84 - 05 Feb 85	-1.689	0.920	-1.547
			515		25 Jan 84 - 05 Feb 85	-0.344	0.880	-1.898
F	-78.108	-174.513	210	567	26 Jan 84 - 04 Feb 85	-4.545	0.318	-1.466
			285		26 Jan 84 - 04 Feb 85	-3.971	0.656	-1.441
G	-78.22	-172.518	215	443	26 Jan 84 - 04 Feb 85	-0.258	-2.477	-1.421
			291		26 Jan 84 - 05 Feb 84	1.556	-1.342	-1.140
			395		26 Jan 84 - 04 Feb 85	-0.246	-3.417	-1.750
H	-78.163	-170.612	228	558	27 Jan 84 - 12 Feb 84	-4.118	-1.362	-1.740
			305		27 Jan 84 - 03 Feb 85	-0.192	-0.316	-1.810
I	-77.68	-160.403	255	590	28 Jan 84 - 02 Feb 85	-1.909	2.198	-1.836
			540		28 Jan 84 - 02 Feb 85	-3.856	5.060	-1.820
L	-78.017	179.767	444	675	26 Jan 78- 18 Aug 78	1.000	1.500	-2.090
Snap	-78.227	-172.49	211	420	05 Feb 83 - 26 Jan 84	0.404	-5.023	-1.508
			283		05 Feb 83 - 26 Jan 84	---	---	-1.528
			383		05 Feb 83 - 26 Jan 84	0.922	-3.622	-1.761
Crackle	-78.183	-174.65	237	530	05 Feb 83 - 26 Jan 84	-8.800	-1.361	-1.419
			310		05 Feb 83 - 25 Jan 84	-8.246	1.851	-1.426
			492		05 Feb 83 - 26 Jan 84	-7.589	-1.226	-1.770
Pop	-78.092	-175.5	253	550	05 Feb 83 - 25 Jan 84	-5.929	-0.437	-1.437
			327		05 Feb 83 - 25 Jan 84	-6.232	-1.431	-1.510
			508		05 Feb 83 - 25 Jan 84	-2.629	1.990	-1.828
Snap 3	-78.192	-172.8	240	436	04 Feb 85 - 10 Nov 86	-1.648	-3.763	-1.420
			315		04 Feb 85 - 21 Apr 86	-3.515	-5.943	-1.323
			390		04 Feb 85 - 11 Feb 87	-1.152	-4.446	-1.671

Mooring Data

All available historical moored time series from near the front of the RIS were used to validate the calculated geostrophic velocities (black x, Figure 3.1). The Pelagic Ross Ice Shelf Moorings (PRISM) experiment (1984-1987) deployed thirteen moorings within 10 km of the front of RIS [*Hellmer and Jacobs*, 1995], each with two to three year-long records of salinity, potential temperature and velocity (Table 3.2). Mean potential temperature and north/south and east/west velocities were calculated for each

of the unfiltered time series. Mean properties for an additional 1978 mooring (L) provided by Pillsbury and Jacobs [1985] are also include in Table 3.2.

Historical Evidence of ISW

Even with a coarse vertical sampling resolution of 100 m, 1936 bottle data (station 78552) in the GCT (colored dots, Figure 3.2) show the characteristics of super-cooled water (yellow line, Figure 3.3a). Farther east, station 78528 (green line) has a stronger ISW signal, likely located along the core, which extends to the shelf break nearly undiluted with θ = -2°C around 400 m deep (station 78530; light blue line). Stations 293574 and 293565 from 1957 (circles, Figure 3.2) show super-cooled water (θ = -2°C) in the GCT at 500 m – 600 m (Figure 3.3c), with the colder ISW characteristic found in the eastern station (293565). In the LAT, a 1956 station (259948; x, Figure 3.2) measured water 0.03°C below the surface freezing point at 200 m deep, likely the result of lateral melting of the RIS rather than basal melt (tan line, Figure 3.3b). A 1960 station (13; stars, Figure 3.2) also measured lateral melt at 230-m along the eastern flank of the LAT with a potential temperature of almost -1.9°C (pink line, Figure 3.3d). Several GCT stations in 1962 (diamonds, Figure 3.2) and 1967 (squares) measured ISW well below (z = 450 m – 500 m) the draft of the RIS (Figure 3.3e-f).

There is no evidence of basal melt signals emerging from under the RIS in the LAT in any of these years. While inconsistencies in the vertical sampling inherent in bottle data could have hindered detection by the 1960 station (stars, Figure 3.2) data, it is also unlikely owing to the mean 35-m vertical sampling resolution and good spatial

station coverage of the LAT (stars, Figure 3.2). Thus, ISW did not likely exist in the LAT before 1967.

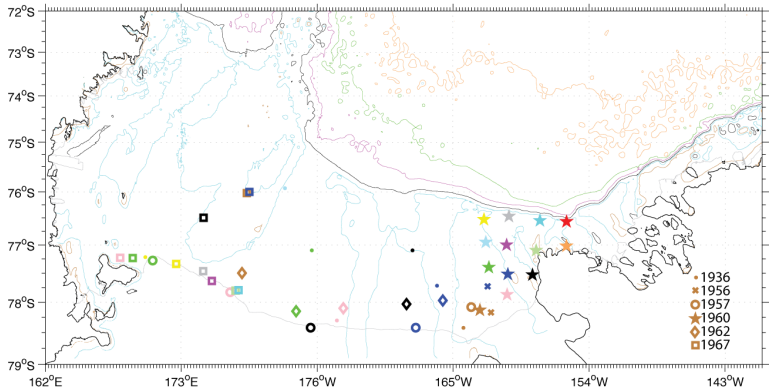

Figure 3.2: Basemap of historical stations from cruises near the RIS. Shown are stations from 1936 (dot), 1956 (x), 1957 (circle), 1960 (star), 1962 (diamond), and 1967 (square). Each color matches the θ-S traces in Figure 3.3.

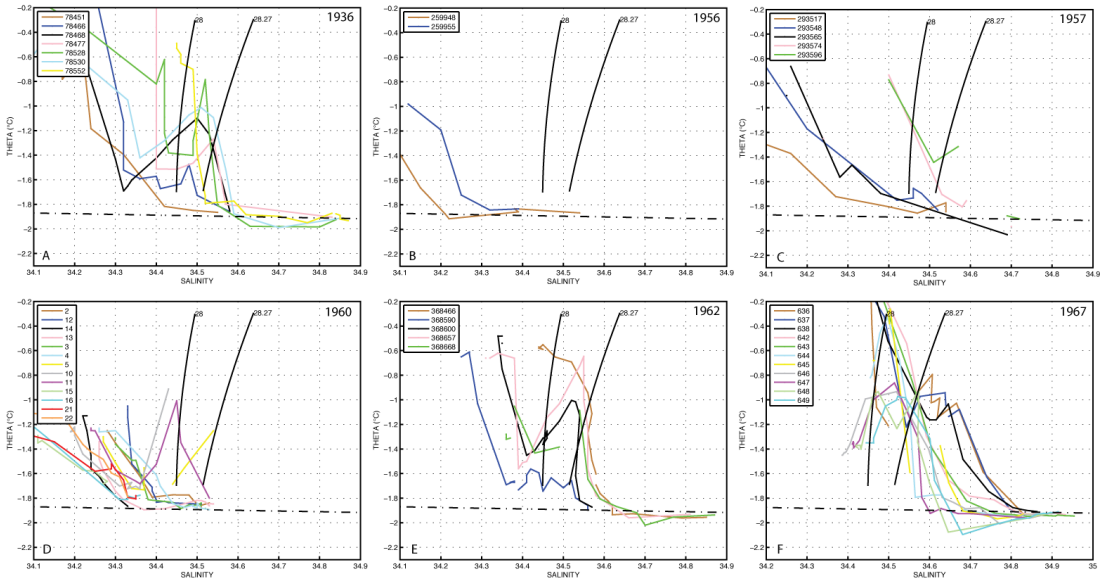

Figure 3.3: Potential temperature versus salinity for historical stations near the RIS. Stations from a) 1936, b) 1956, c) 1957, d) 1960, e) 1962, and f) 1967 are shown. The locations of these stations can be found in Figure 3.2.

Evolving Characteristics at the RIS Front

Comparison of the five synoptic CTD transects reveals ongoing water mass changes in front of the RIS. In 1976, a 100-km wide inflow of MCDW ($\theta > -1.0°C$) is found between 125 m and 300 m directly over Hayes Bank (Figure 3.4) with potential temperature reaching nearly -0.8°C (Figure 3.5) and a mean salinity of 34.5. In 1984, this weaker warm core ($\theta > -1.2°C$) is split into two cores and shifted slightly to the west (Figures 3.6 and 3.7). Less pronounced MCDW, i.e. fresher ($\Delta S = -0.05$), colder ($\Delta\theta = -0.7°C$), and thinner, than in previous years is found in the 1994 section (Figures 3.8 and 3.9). In 2000, the warmest inflow ($\theta > -1.45°C$) is approximately 50 m deeper in the water column than in previous years (Figures 3.10 and 3.11). This core deepening continues into 2007 where the noticeably colder MCDW ($\theta > -1.6°C$) is found at 350 m, i.e. about 100 m deeper than in 1976 (Figures 3.12 and 3.13). The reported MCDW waning by JG10 is also evident by the thinning of this core to about half of its original 1976 size by 2007.

ISW in the GCT, although showing some decadal variability, has remained relatively constant in size and location. Water with potential temperature colder than -2.0°C is typically found at about 450 m. This 150-km wide plume in 1976 was extremely dense ($\gamma^n > 28.6$ kg m^{-3}) and relatively salty ($S \approx 34.66 – 34.8$) (Figures 3.4 and 3.5). A smaller and warmer ($\theta < -1.95°C$) plume of equally dense and salty water is seen in the western GCT around 500 m, likely a remnant of a return flow from the main core. Slightly less salty (Figures 3.6 and 3.7) ISW in 1984 shoaled to near 250 m (Figure 3.6), and two relatively smaller western return flows of ISW are found 400 m and 250 m

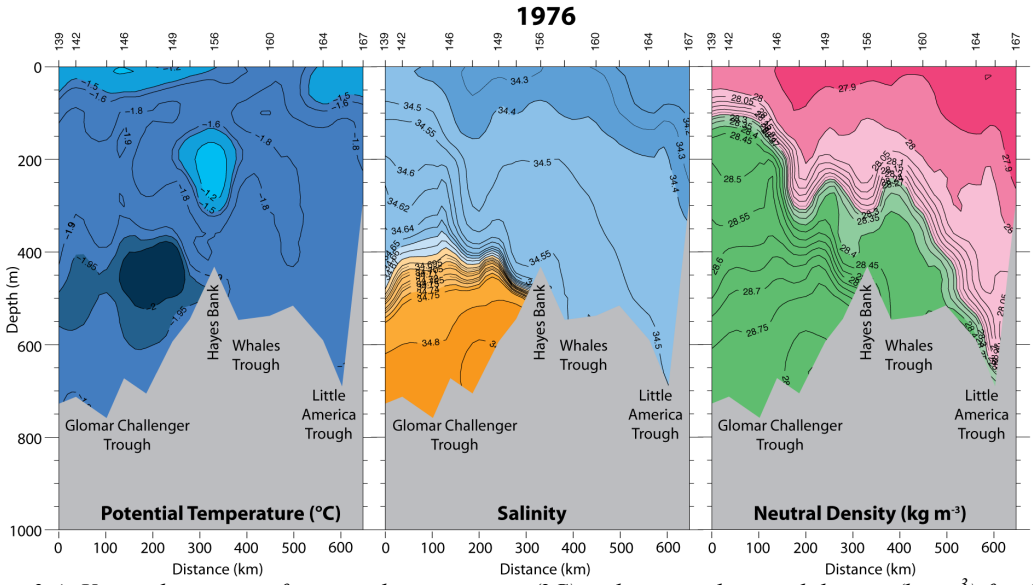

Figure 3.4: Vertical sections of potential temperature (°C), salinity, and neutral density (kg m^{-3}) for the 1976 section at the RIS.

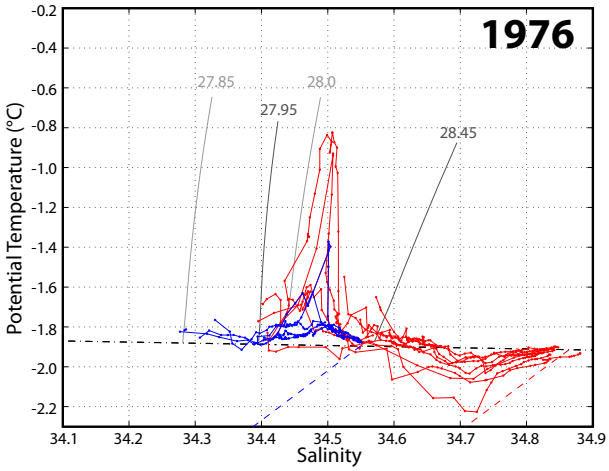

Figure 3.5: Potential temperature versus salinity for 1976 stations along the RIS below the temperature minimum. Red (blue) stations are found west (east) of Hayes Bank. The black dashed line shows the temperature of the freezing point at the surface. Colored dashed lines correspond to the Gade Line. Isoypcnals used for the zero reference level and for the temperature minimum are shown by the dark (light) grey lines for west (east) of Hayes Bank.

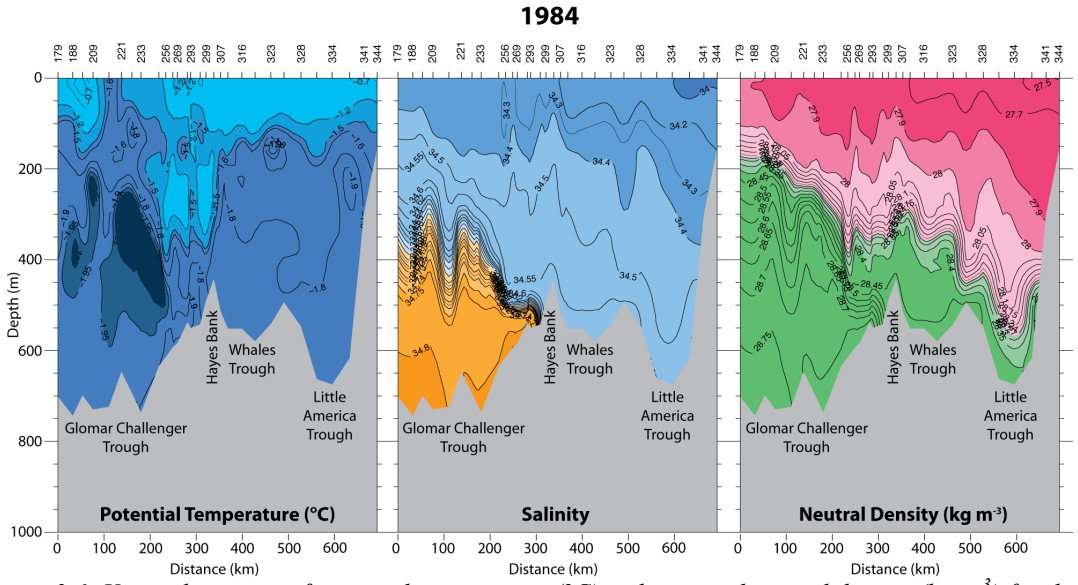

Figure 3.6: Vertical sections of potential temperature (°C), salinity, and neutral density (kg m^{-3}) for the 1984 section at the RIS.

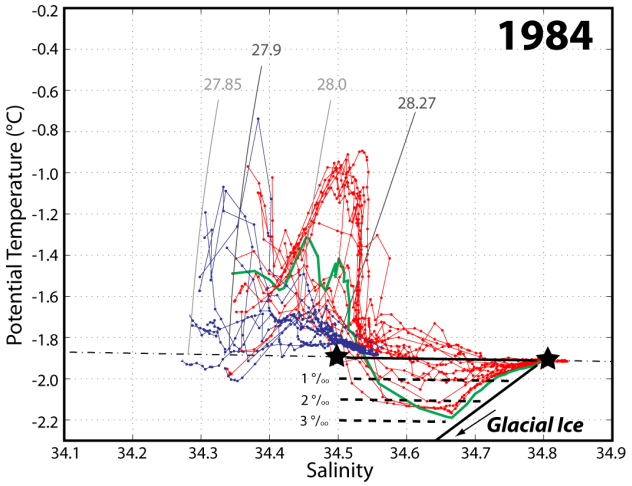

Figure 3.7: Potential temperature versus salinity for 1984 stations along the RIS below the temperature minimum. Red (blue) stations are found west (east) of Hayes Bank. The black dashed line shows the temperature of the freezing point at the surface. Isoypcnals used for the zero reference level and for the temperature minimum are shown by the dark (light) grey lines for west (east) of Hayes Bank. Black stars show example end members A and B from equation (1) with dashed lines of equal melt water concentrations.

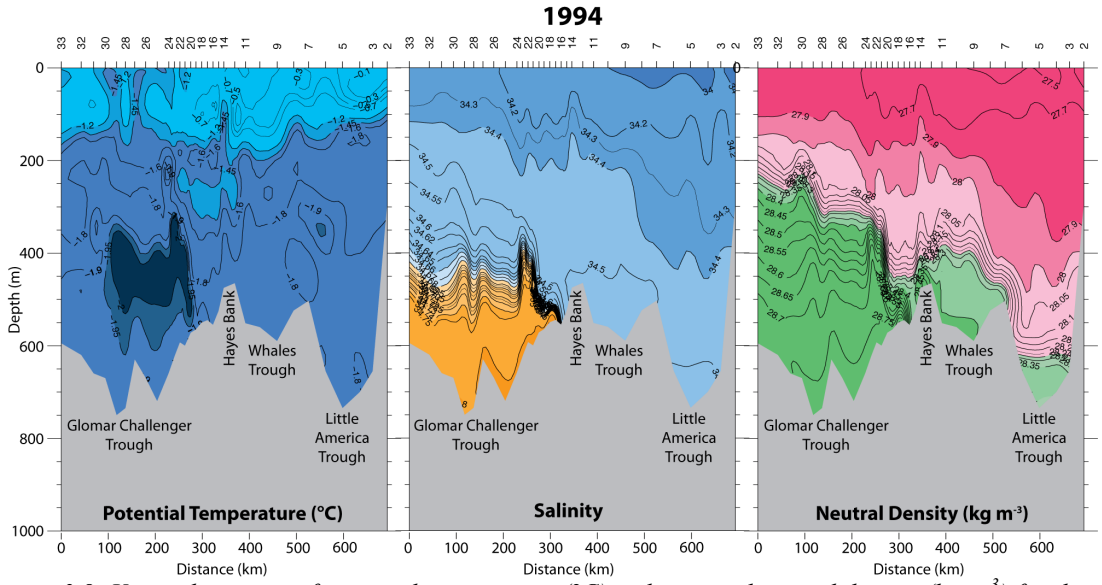

Figure 3.8: Vertical sections of potential temperature (°C), salinity, and neutral density (kg m^{-3}) for the 1994 section at the RIS.

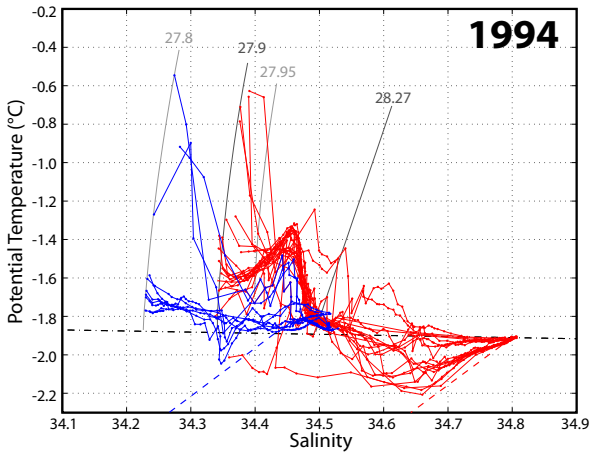

Figure 3.9: Potential temperature versus salinity for 1994 stations along the RIS below the temperature minimum. Red (blue) stations are found west (east) of Hayes Bank. The black dashed line shows the temperature of the freezing point at the surface. Colored dashed lines correspond to the Gade Line. Isoypcnals used for the zero reference level and for the temperature minimum are shown by the dark (light) grey lines for west (east) of Hayes Bank.

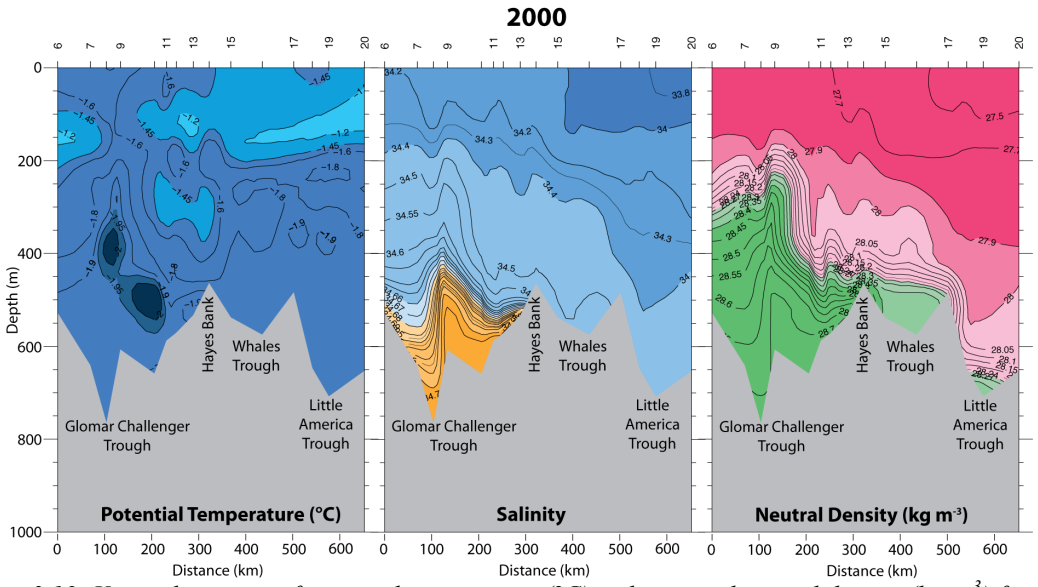

Figure 3.10: Vertical sections of potential temperature (°C), salinity, and neutral density (kg m^{-3}) for the 2000 section at the RIS.

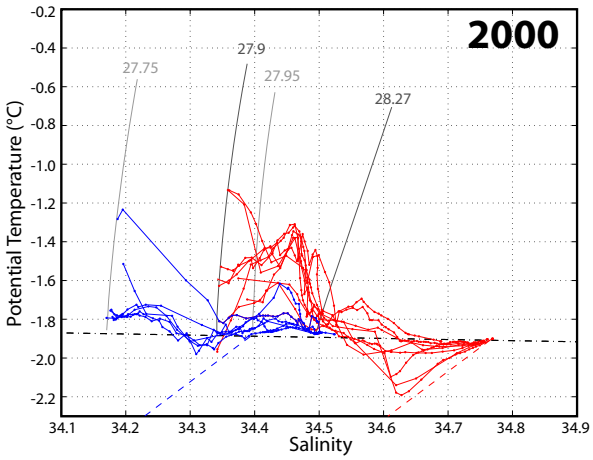

Figure 3.11: Potential temperature versus salinity for 2000 stations along the RIS below the temperature minimum. Red (blue) stations are found west (east) of Hayes Bank. The black dashed line shows the temperature of the freezing point at the surface. Colored dashed lines correspond to the Gade Line. Isoypcnals used for the zero reference level and for the temperature minimum are shown by the dark (light) grey lines for west (east) of Hayes Bank.

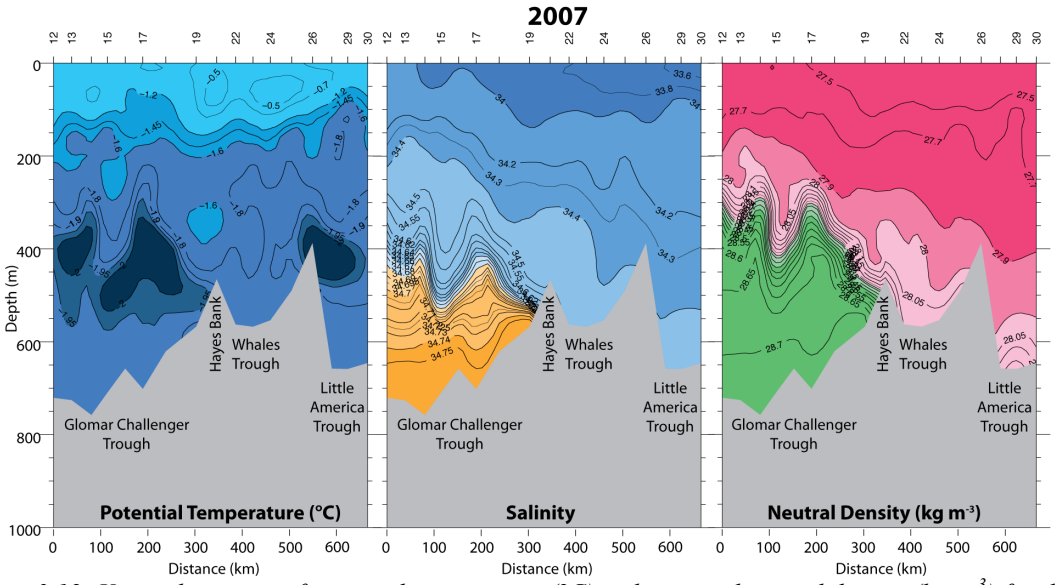

Figure 3.12: Vertical sections of potential temperature (°C), salinity, and neutral density (kg m^{-3}) for the 2007 section at the RIS.

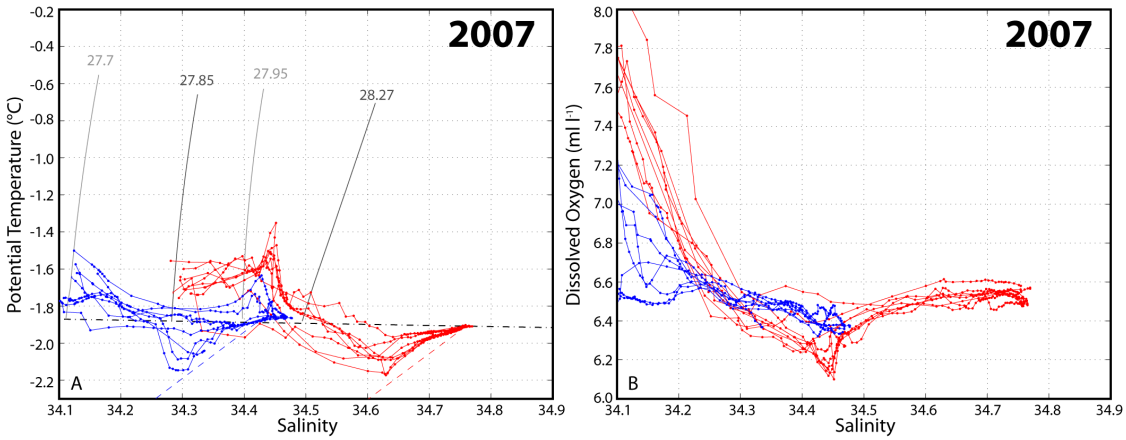

Figure 3.13: Potential temperature versus salinity and salinity versus oxygen for 2007 stations along the RIS below the temperature minimum. Red (blue) stations are found west (east) of Hayes Bank. a) The black dashed line shows the temperature of the freezing point at the surface. Colored dashed lines correspond to the Gade Line. Isoypcnals used for the zero reference level and for the temperature minimum are shown by the dark (light) grey lines for west (east) of Hayes Bank.

respectively. Along the eastern flank of the LAT, an additional shallow (z = 250 m) patch of relatively fresh (S ≈ 34.35) super-cooled (θ < -1.9°C) water is observed. Although not dense enough (γ^n < 27.95 kg m^{-3}) to be classified as ISW, this is indicative of interaction with the RIS through either basal or lateral melt.

The 1994 θ-S properties of ISW (Figure 3.8; 3.9) are nearly identical to those in 1984. Found slightly deeper in the water column, the 1994 plume is about 50 km wider (Figure 3.8). A relatively fresh (S = 34.35) secondary outflow (θ < -1.9°C) is also found over the western flank of the LAT, but it is deep enough (z = 350 m) to have originated from under the RIS. In 2000, two ISW cores are seen in each the GCT (θ < -2°C; 375 m and 475 m deep) and the LAT (θ < -1.9°C; 350 m deep) (Figure 3.10), and are slightly fresher (ΔS = -0.03) than in 1994 (Figure 3.11).

In 2007 two cores with potential temperatures near -2.2°C at 400 m in the GCT (Figure 3.12) have salinities almost equal to that of 2000 (Figure 3.13a). Farther east in the LAT, a substantially larger area of relatively fresh (S = 34.3) super-cooled water has potential temperatures (θ < -2°C) as cold as the GCT outflow (Figure 3.12).

Determining the percent of RIS glacial melt water (melt water fraction) in ISW and the associated volume transport will help in the quantification of observed ongoing variability in super-cooled water characteristics. Shallow lateral mixtures (z < 200 m) containing some mixture of melt water will also be included in this study calculations.

Melt Water Fraction

ISW in the Ross Sea is typically injected into the SW layer between LSSW (B) and HSSW (A) (stars; Figure 3.7). Following a three-member mixing scheme of Jenkins

[1999] and Jenkins and Jacobs [2008], if more than one tracer is available, e.g. salinity and temperature, a composite of two tracers is:

$$\psi_{mix} = (\chi^2_{mix} - \chi^2_A) - (\chi^1_{mix} - \chi^1_A)\left(\frac{\chi^2_B - \chi^2_A}{\chi^1_B - \chi^1_A}\right) (1a)$$

$$\psi_{melt} = (\chi^2_{melt} - \chi^2_A) - (\chi^1_{melt} - \chi^1_A)\left(\frac{\chi^2_B - \chi^2_A}{\chi^1_B - \chi^1_A}\right) (1b)$$

where $\chi^{2,1}{}_{A,B}$ are characteristic values of each water mass found at the front of the ice shelf with the straight line in between defining the zero melt water concentration. $\chi^{2,1}{}_{melt}$ is pure glacial melt water (S = 0) and $\chi^{2,1}{}_{mix}$ is the CTD profile data. The melt water fraction is estimated as:

$$\varphi = \frac{\psi_{mix}}{\psi_{melt}} (2)$$

For the HSSW end member the mean near-freezing bottom salinity for each year is used. The LSSW end member is a fresher salinity than ISW at the surface freezing point temperature. When this HSSW mixes with pure glacial melt water it produces a melt water mixture (*MWM*) that based on a given salinity S_{MWM} will have temperature T_{MWM} [*Gade*, 1979; *Jenkins*, 1999; *Wahlin et al.*, 2010]:

$$T_{MWM}(S_{MWM}) = T_A + \frac{L_f}{c_p}\left(1 - \frac{S_A}{S_{MWM}}\right) (3)$$

where T_A and S_A are the mean temperature and salinity of HSSW; L_f is the latent heat of melting for ice; and c_p is the specific heat of seawater with a salinity of S_A, temperature of T_A, and pressure of 500 db, the average depth of the Ross Sea. Equation (3) represents the Gade Line (Figure 3.7), which when extrapolated to a zero salinity for all five years

has an effective potential temperature [*Hellmer et al.*, 1998; *Jenkins*, 1999; *Jenkins and Jacobs*, 2008] of -87.5°C to -89.9°C, with a mean of -88°C. A mean ice temperature of -5°C can produce an effective potential ice temperature of -89.2°C, which is within the range above. Ice temperatures of this magnitude were measured directly within the bottom 50 m of the RIS through the J-9 drill site (82° 22'S, 168° 37'W) [*Clough and Hansen*, 1979], thus is a realistic estimate for the glacial ice end member.

Previous estimates of melt water fraction in front of the George VI Ice Shelf [*Jenkins and Jacobs*, 2008] and PIG [*Jacobs et al.*, 2011; *Jenkins*, 1999] tested three different tracer pairs: θ/S, θ/O_2, and S/O_2. The S/O_2 fractions were deemed the most reliable. A clear low-oxygen signal from the CDW is found in those two regions thus an appropriate oxygen end member for glacial ice can be estimated. However, because ISW is formed from "new" SW, $S\text{-}O_2$ plots do not show any apparent low signal in the super-cooled water (Figure 3.13b) west (east) of Hayes Bank for salinities of approximately 34.62 (34.30). The most distinguishable signal is from the low-oxygen core of MCDW ($S \approx 34.45$, $O_2 < 6.2$ ml l^{-1}). Therefore, the melt water fraction calculation at the RIS is best-computed using temperature and salinity as the tracers.

Evolving SW salinities over time dictate that unique water mass end members are needed for each year. A listing of the temperature and salinity values used for end-members A and B as well as glacial ice are found in Table 3.3. For simplicity we assume that the temperature of glacial ice remains the same for all years and is consistent throughout the entire basal side of the RIS.

Table 3.3. List of tracer end members used in melt water fraction calculation.

	Glomar Challenger				Little America				Glacial Ice	
Year	**End Member A**		**End Member B**		**End Member A**		**End Member B**			
	S	θ	S	θ	S	θ	S	θ	S	θ
1976	34.88	-1.915	34.35	-1.885	34.55	-1.895	34.35	-1.885	0	-88
1984	34.80	-1.910	34.30	-1.882	34.42	-1.890	34.25	-1.880	0	-88
1994	34.80	-1.910	34.25	-1.879	34.43	-1.890	34.20	-1.875	0	-88
2000	34.77	-1.908	34.20	-1.876	34.40	-1.890	34.25	-1.880	0	-88
2007	34.76	-1.908	34.30	-1.882	34.42	-1.890	34.15	-1.870	0	-88

Adjusted Geostrophic Velocity Methods

In the absence of direct current measurements concurrent with our five years of CTD data, geostrophic velocities were calculated for each section. Reference levels were chosen with respect to carefully selected isopycnals dividing the main cores of inflowing MCDW and outflowing ISW (Table 3.4). Different reference levels were chosen for the eastern and western Ross Sea each year due to the two different varieties of ISW. Hayes Bank serves as a logical division between the two regimes because it is the shallowest ($z < 450$ m) of the three dividing banks along the RIS, thus impedes the eastward spread of the saltiest variety of SW. Therefore, ISW produced west (east) of this Bank is likely

Table 3.4. Selected neutral density surfaces used as reference levels east and west of Hayes Bank (HB) for geostrophic velocity calculations and mean neutral density of temperature minimum.

	γ^n Reference Level (kg m^{-3})		γ^n of T_{min} (kg m^{-3})	
Year	**west of HB**	**east of HB**	**west of HB**	**east of HB**
1976	28.45	28.00	27.95	27.85
1984	28.27	28.00	27.95	27.85
1994	28.27	27.95	27.90	27.80
2000	28.27	27.95	27.90	27.75
2007	28.27	27.95	27.85	27.70

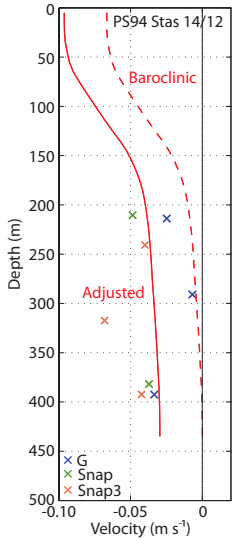

Figure 3.14: Example of velocity adjustment using all available mooring data found between a station pair. The derived geostrophic velocity (dashed line) is adjusted (solid line) using the minimum RMS error of all the available current meter records (colored x).

derived from saltier (fresher) SW. In instances where the warm core spreads eastward past the apex of Hayes Bank, the transition between reference levels is shifted one additional station pair to not separate this inflow. Velocity profiles for station pairs in which a historical mooring fell in between were adjusted using the minimum RMS error to the record-length mean mooring velocity normal to the section (see Figure 3.14 for an example) then linearly interpolated for those pairs lacking a historical mooring.

The constructed geostrophic fields do not guarantee that water masses of a known origin end up with flow in the appropriate direction (e.g. southward flowing warm core) or that these sections which span almost the entire RIS conserve mass and tracers within the cavity. Following the methods of Wunsch [1978] and Jenkins and Jacobs [2008] the mass and tracers transport across these sections were balanced by an

inverse method to derive a reference (”barotropic”) velocity (v) at each station pair location:

$$v = W^{-1} A^T (A W^{-1} A^T)^{-1} (-b) \qquad (4)$$

where:

$$A_{ij} = \frac{1}{g}\left\{\int_{P_{bot}}^{P_{top}} [\chi_i(p) - \chi_{melt}]\Delta x(p)dp\right\}_j \quad (5)$$

$$b_i = \frac{1}{g}\left\{\int_{P_{bot}}^{P_{top}} v_{BC}(p)[\chi_i(p) - \chi_{melt}]\Delta x(p)dp\right\}_j \quad (6)$$

$$v_j = (v_{BT})_j \quad (7)$$

where P is pressure, χ_i is the mean property values for the station pair, χ_{melt} is the melt water property end member used in Equation (2), v_{BC} is the baroclinic velocity derived from station data, Δx is the distance between the station pair and v_{BT} is the desired barotropic velocity. Columns of A are area weighted (W_{jj}) to avoided any potential biases with unevenly spaced stations:

$$W_{jj} = \frac{\frac{1}{g}\left\{\int_{P_{bot}}^{P_{top}} \Delta x(p)dp\right\}_j}{\sum \frac{1}{g}\left\{\int_{P_{bot}}^{P_{top}} \Delta x(p)dp\right\}_j} \quad (8)$$

The integrals in (5), (6), and (8) can be used over the entire water column, from P_{top} to $P_{bot(tom)}$, or as for the case in this study, over portions of the water column unaffected by surface influences that can likely alter the profile data, i.e. we excluded water from the surface to the base of the temperature minimum. A listing of the

temperature minimum for each year can be found in Table 3.4. The resulting reference velocity was added to the geostrophic velocity to get the adjusted geostrophic transport.

Results

Melt Water Fraction

Vertical sections of the calculated melt water fraction ($^{o}/_{oo}$) for each year are shown in Figure 3.15. Melt water in the GCT, although showing some variability, is found in roughly the same location each year. Patches of lateral melt shallower than 200 m are found scattered throughout the vertical sections, with the exception of 2007 where no lateral melt was measured. In the LAT, melt water was not present until after 1984. This plume progressively deepens until 2007 where it occupies a larger area with a melt water fraction more like GCT characteristics. While an increase in the area of melt water mixtures might be indicated (Table 3.5), little can be said about whether this is due to an increase in the production of ISW. These melt water fractions when combined with the adjusted geostrophic volume transports yield export of melt water for each of the five years.

Table 3.5. Vertical area (km^2) of water with a melt water fraction greater than 0.4 ppt for the GCT, LAT, and total section for each year. Areas do not include lateral melt water.

	Vertical Area (km^2)		
Year	**Glomar Challenger**	**Little America**	**Total**
1976	46.12	0	46.12
1984	51.98	3.10	55.08
1994	43.92	3.50	42.47
2000	19.46	4.51	23.97
2007	63.36	17.63	80.99

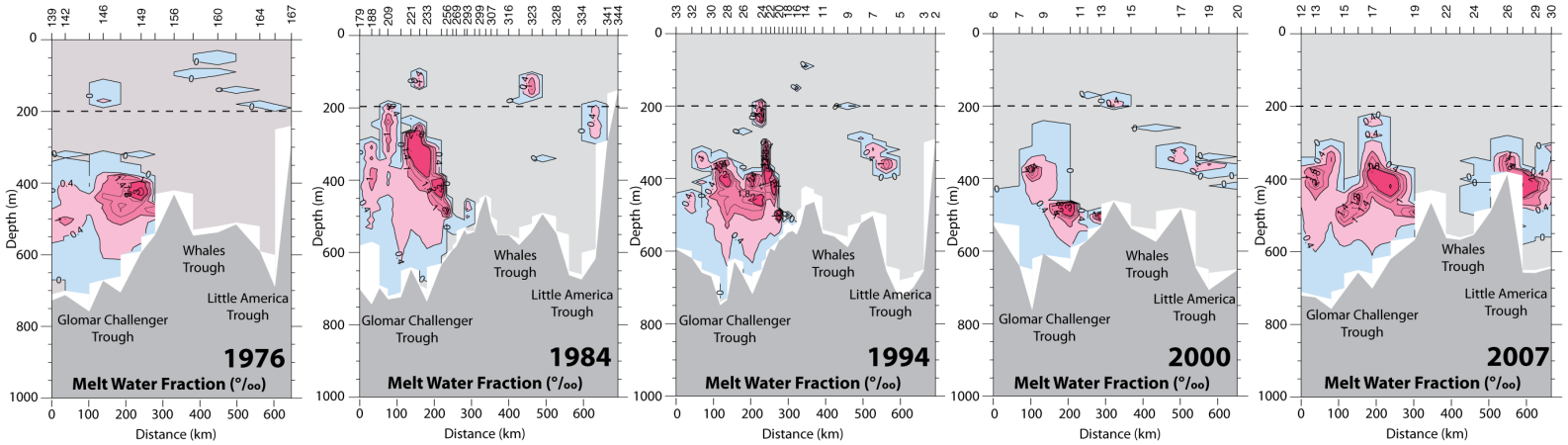

Figure 3.15: Vertical sections of melt water fraction in parts per thousand (°/₀₀). Dark (light) grey shades show the bottom topography (zero melt water fraction).

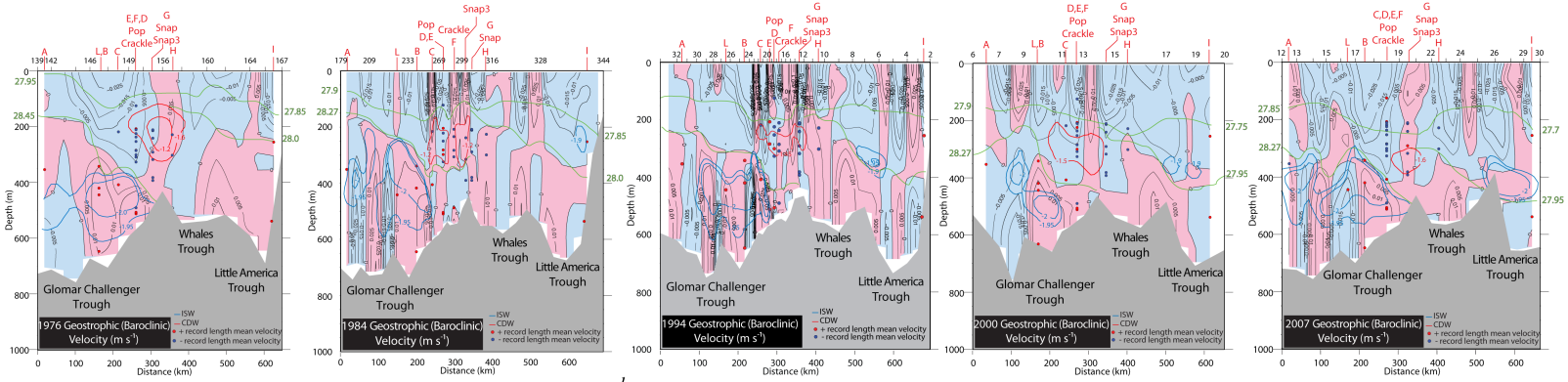

Figure 3.16: Vertical sections of geostrophic velocity (m s^{-1}). Northward (southward) velocities correspond to pink (blue) shades. Red (blue) contours of potential temperature are of the main core of MCDW (ISW). Red (blue) dots are record-length mean northward (southward) velocities from the historical moorings listed in Table 3.2. Green traces show the position of the isopycnal used for the reference level and the temperature minimum listed in Table 3.4.

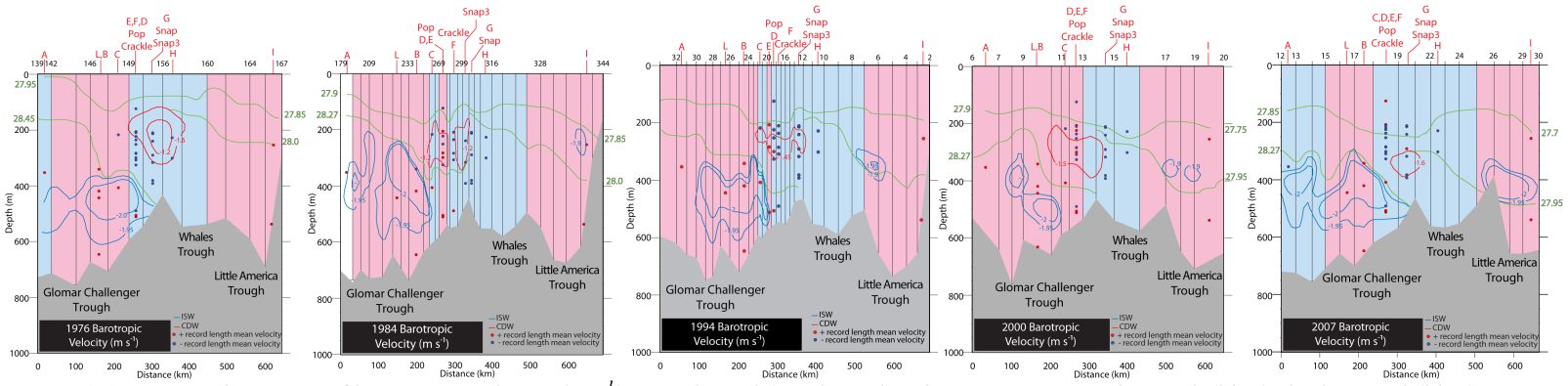

Figure 3.17: Vertical sections of barotropic velocity (m s^{-1}). Northward (southward) velocities correspond to pink (blue) shades. Red (blue) contours of potential temperature are of the main core of MCDW (ISW). Red (blue) dots are record-length mean northward (southward) velocities from the historical moorings listed in Table 3.2. Green traces show the position of the isopycnal used for the reference level and the temperature minimum listed in Table 3.4.

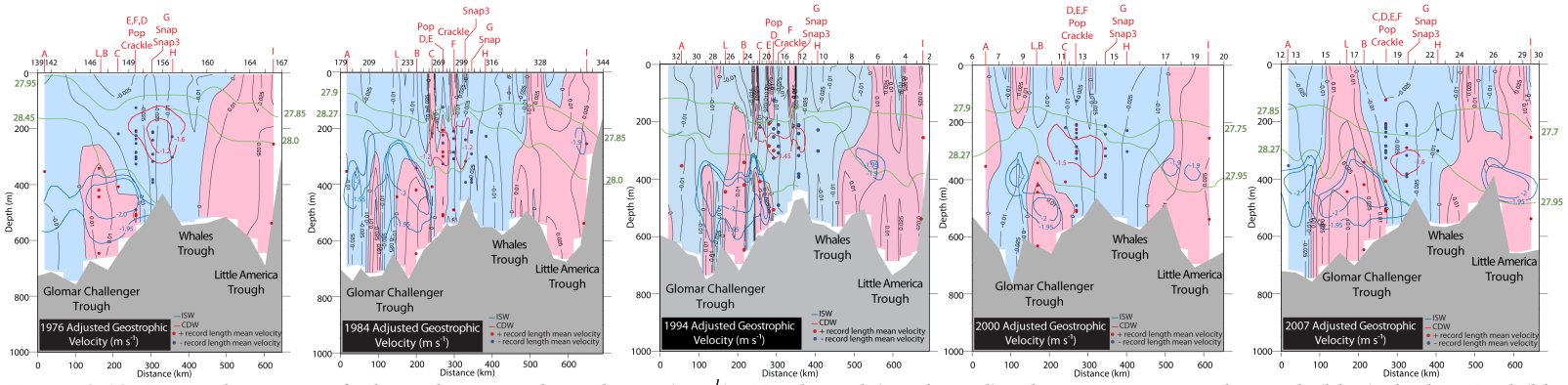

Figure 3.18: Vertical sections of adjusted geostrophic velocity (m s^{-1}). Northward (southward) velocities correspond to pink (blue) shades. Red (blue) contours of potential temperature are of the main core of MCDW (ISW). Red (blue) dots are record-length mean northward (southward) velocities from the historical moorings listed in Table 3.2. Green traces show the position of the isopycnal used for the reference level and the temperature minimum listed in Table 3.4.

Velocities

Geostrophic (barotropic) velocities are shown in Figure 3.16 (3.17). Table 3.6 lists the mean and maximum northward and southward barotropic velocities for each year. The same general pattern of northward velocities in the interior of the GCT and LAT and southward flow along the eastern flank of the GCT and Whales Trough is consistent in all five years. A few exceptions to this pattern occur in 1976 and 2007 with southward velocities in the western GCT. For all cases, the maximum poleward velocity is over Hayes Bank, while the maximum northward is found at the easternmost station pair, with the exception of 2007 when it is found in the middle of the GCT. While these extremes rarely exceed ± 4 cm s^{-1}, the mean barotropic velocities are fairly consistent from year to year and in all but one case (2000) are smaller than ±1.6 cm s^{-1}.

The final adjusted geostrophic velocities show a very consistent pattern for each RIS section (Figure 3.18). MCDW persists as a relatively strong (>2.5 cm s^{-1}) southward core typically either west of Hayes Bank (1976 and 2007) or centered directly over it (1984, 1994, and 2000). While the temperature of this inflow appears to be waning, the intensity of its southward transit remains fairly consistent over the 30 years.

Table 3.6. Mean and maximum barotropic velocities from mooring adjustment and inverse box model for each RIS section.

	Mean (m s^{-1})		**Maximum (m s^{-1})**	
Year	**Northward**	**Southward**	**Northward**	**Southward**
1976	0.0109	-0.0135	0.0240	-0.0380
1984	0.0085	-0.0147	0.0308	-0.0490
1994	0.0104	-0.0134	0.0270	-0.0340
2000	0.0121	-0.0209	0.0320	-0.0340
2007	0.0156	-0.0151	0.0320	-0.0380

In the GCT, ISW outflows are relatively strong (> 2.5 cm s^{-1}) during three (1984, 1994, and 2007) of the five years, with weaker (>1 cm s^{-1}) outflows in 1976 and 2000. Southward ISW cores when present have speeds equal to their northward component. Closer station spacing along the GCT in 1984 and 1994 (Table 3.1) reveals a more detailed structure of banded ISW velocity reversals. In the LAT, melt water outflows maintain a relatively constant velocity > 1 cm s^{-1}, with the exception of a slightly weaker 1994. Over the 31 years, when comparing the overall circulation pattern from year to year there is no apparent increase or decrease in velocities.

Ross Ice Shelf Cavity Residence Times

The adjusted volume transports are used to inspect the residence times of the RIS cavity (125,300 km^3) [*Smethie and Jacobs*, 2005]. The net southward transport below the temperature minimum yields the residence times found in Table 3.7. These values vary slightly from year to year with the shortest residence time in 2007. Previous estimates of RIS cavity residence times using CFC ages for 1994 and 2000 were 4.8 years and 4.1 years respectively [*Smethie and Jacobs*, 2005]. These residence times would require a total southward flowing volume transport 50 percent less than those reported here: 0.83 Sv (1994) and 0.97 Sv (2000). Even longer residence times were calculated by Loose et al. [2009] as 7.5 years (1994) and 5.5 years (2000), equivalent to a total southward volume transport of 0.53 Sv and 0.72 Sv, respectively. If we assume a mean entrance to the cavity is 750 km long and a mean depth of 550 m, the area of water below the 200-m draft of the RIS is 262 km^2. The longer residence time for both years would require a mean northward velocity less than 0.4 cm s^{-1}. The same cross sectional

area using our residence times would require a mean velocity of 1 cm s^{-1}, a more realistic estimate given that the mean northward velocity from the historical moorings is 1.7 cm s^{-1} (Table 3.2).

Table 3.7. Total northward transport and residence times for the RIS cavity for each year using the adjusted volume transports below the temperature minimum.

Year	Total Northward Transport (10^6 m^3 s^{-1})	Cavity Residence Time
1976	2.08	1.91 years
1984	2.39	1.66 years
1994	2.13	1.86 years
2000	1.83	2.16 years
2007	2.40	1.65 years

Melt Water Transport

Melt water transports (km^3 of freshwater per year) are calculated as the product of the adjusted volume transports and the melt water fraction (Table 3.8). With the exception of 1984, the GCT melt water transport from 1976 until 2000 remained relatively constant with outflows around 5 km^3 a^{-1}. Likewise, when melt water was present, the LAT showed the same consistency up to 2000, but an order of magnitude smaller. From 2000 to 2007, melt water transport drastically increased to three times larger in the GCT, and an even more remarkably 25 times larger in the LAT. The relatively consistent velocity from 2000 – 2007 indicates that this increase is largely due to the growing cross sectional area of melt water. Overall, the GCT has an increasing trend in melt water transport of 1.3 km^3 per decade, with an increase of 6.8 km^3 per decade from 2000 to 2007. The LAT had a more dramatic increase of 2.6 km^3 per

Table 3.8. Net volume transport (10^6 m^3 s^{-1}) and net melt water transport (km^3 a^{-1}) for each year from the temperature minimum to the bottom for the entire RIS front (total), GCT and LAT.

Year	Net Transport (10^6 m^3 s^{-1}) East of 173°E (full RIS)	Net Melt Water Transport (km^3 a^{-1})		
		Total	GCT	LAT
1976	0.0032 (0.0041)	4.85	4.85	0.00
1984	0.0024 (0.0044)	0.16	0.16	0.00
1994	0.0031 (0.0043)	5.90	5.43	0.47
2000	0.0025 (0.0025)	4.00	3.60	0.40
2007	0.0025 (0.0032)	19.25	8.36	10.89

Table 3.9. Selected neutral density surfaces used as reference levels for geostrophic velocity calculations and mean neutral density of temperature minimum for each Amundsen Sea ice shelf.

Ice Shelf	γ^n Reference Level (kg m^{-3})	γ^n of T_{min} (kg m^{-3})
PIG	27.9	27.6
Dotson	27.9	27.6
Getz	27.95	27.7

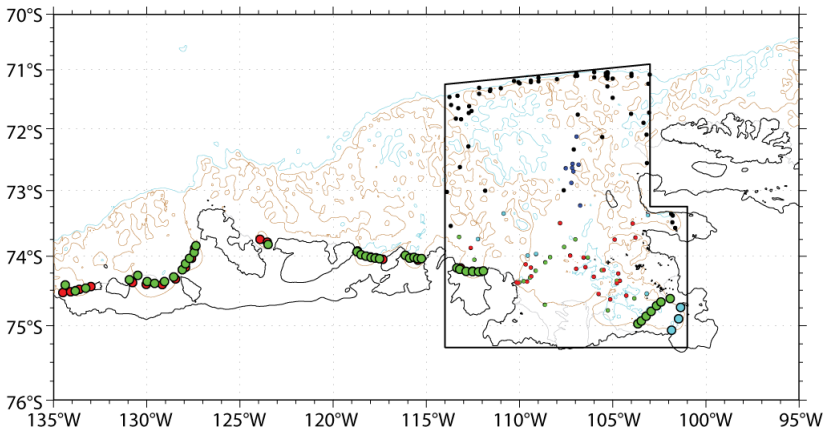

Figure 3.19: Location of stations used to estimate the melt water transports for the Amundsen Sea. Stations used from 1994 (cyan), 2000 (red), and 2007 (green) are outlined in black. Stations west (east) of 115°W (105°W) are considered Getz Ice Shelf (PIG) and between 115°W and 111°W considered Dotson Ice Shelf. The area used to estimate the volume of AASW within the Amundsen Sea is enclosed by the black box. The colored dots within are the locations of stations from 1994-2010 (blue) used in Figure 7.4. Black dots show the remaining historical stations in the area.

decade from 1976 to 2007, and like the GCT, the largest from 2000 to 2007 at a rate of 14.9 km^3 per decade.

Upstream Sources

Data from the Amundsen Sea in front of the PIG and the Getz and Dotson Ice sheets were also used to determine changing melt water sources upstream of the Ross Sea. Two cruises in 1994 and 2007 collected station data in front or very near the PIG (Figure 3.19). Additionally, a cruise in 2000 collected CTD data in front of the Getz and Dotson ice shelves. Due to the lack of Shelf Water in this region, melt water fraction end members A and B are CDW and Winter Water, respectively. Geostrophic velocities were calculated using reference levels (Table 3.9) indicative of the temperature maximum slightly north of the ice shelf front. The volume and property fluxes were then balanced below the temperature minimum (Table 3.9) by the inverse method. Melt water transports were then calculated (Table 3.10).

Previous calculations of melt water transport for the PIG using a more subjective reference level and surface layer estimated 57 $km^3\ a^{-1}$ in 1994 and 79.4 $km^3\ a^{-1}$ of melt water in 2009 [*Jacobs et al.,* [2011]. At the time of this study, the 2009 data was not publically available, thus the 2007 stations collected slightly north of the 1994 data are used (Figure 3.19). Although the new melt water transports calculated here are slightly smaller, they show an increase in melt water input of the same magnitude. Thus our new estimates indicate an increase in the PIG's melt water export at a rate of 1.77 $km^3\ a^{-1}$ compared to Jacobs et al. [2011] increase of 1.49 $km^3\ a^{-1}$. The Dotson glacier has an increase of melt water transport (1.48 $km^3\ a^{-1}$) only slightly less than that of the PIG.

However, the Getz Glacier does not contribute much new melt water. The transport calculations allow for ambient melt water to flow under the ice sheets, thus a negative trend could result from PIG and Dotson melt water injected downstream, making its way under the Getz. Poor station coverage of the six separated ice fronts could also potentially underestimate new outflows. Without (with) the inclusion of the Getz, there is an estimated 3.25 (1.98) $km^3\ a^{-1}$ increase of new melt water with Amundsen Sea origin.

Table 3.10. Net transport ($km^3\ a^{-1}$) for each year from the temperature minimum to the bottom for the PIG, Dotson and Getz ice shelves.

	Melt Water Transport ($km^3\ a^{-1}$)		
Year	**PIG**	**Dotson**	**Getz**
1994	49.06	--	--
2000	--	20.15	3.86
2007	72.12	30.51	-5.06
Rate of Change	+1.77	+1.48	-1.27

Discussion

Past studies tried to estimate the steady state basal melt rate of the RIS using either modeled results or sparse data with many assumptions (Table 3.11) [*Assmann et al.*, 2003; *Hellmer and Jacobs*, 1994; 1995; *Holland et al.*, 2003; *Horgan et al.*, 2011; *Jacobs et al.*, 1979; *Jacobs et al.*, 1996; *Jacobs et al.*, 1992; *Pillsbury and Jacobs*, 1985; *Shabtaie and Bentley*, 1987; *Smethie and Jacobs*, 2005; *Trumbore et al.*, 1991]. However, few studies have looked at changes occurring in this basal melting. Loose et al. [2009] estimated a glacial melt water flux across the RIS front for two different years from multiple tracers (θ, S, δO^{18}, Ne, ^4He, and O_2) using optimal multiparameter

analysis. A RIS cavity residence time derived from CFC age, in conjunction with the estimated volume of water within the cavity, yielded a melt water flux of 33 km^3 a^{-1} in 1994 and 50 km^3 a^{-1} in 2000. Smethie and Jacobs [2005] using CFCs and salinity calculated average melt rates for these same years of 33 km^3 a^{-1} (1994) and 43 km^3 a^{-1} (2000). In both studies the melt water fluxes are an order of magnitude larger than our 1994 and 2000 values. While it is hard to indicate any sort of a trend from just two melt rate estimates, if we were to assume the increase in basal melt reported in these studies were long-term, it would yield a melt water transport anomaly of 1.66 km^3 a^{-1} [*Smethie and Jacobs*, 2005] and 2.83 km^3 a^{-1} [*Loose et al.*, 2009].

Our 1994 and 2000 estimates do not show an increase at this rate, but rather a decrease of -0.3 km^3 a^{-1}. However, the sharp increase in melt water transports from 2000 to 2007 of 2.17 km^3 a^{-1} falls within the same range as the previous studies. In the LAT, although the magnitude of melt water transport for each year is much smaller than that calculated for the PIG, after 2000 melt water inputs for both regions are increasing at the same rate, with the RIS LAT melt water having a more direct effect on freshening the Ross Sea AASW.

Using a high-resolution climatology for the Ross Sea [OW09; S06], we can estimate the exact freshening induced from these increasing melt water transports. The climatology mean properties most closely match 1992 measured values reported by JG10. SW in the Ross Sea has a volume weighted mean salinity of 34.71. If this volume (1.14×10^5 km^3) were continuously freshened by the increasing GCT melt water after 2000, it would be freshened to 34.70 in 2011, a decrease of this entire layer

Table 3.11. Basal melt rates for the RIS reported in the literature.

Paper	Reported RIS melt rate ($km^3\ a^{-1}$)
Jacobs et al. [1979]*	83
Pillsbury and Jacobs [1985]	73
Shabtaie and Bentley [1987]	60
Trumbore et al. [1991]	79
Jacobs et al. [1992]*	73
Hellmer and Jacobs [1994]*	59-89
Hellmer and Jacobs [1995]	17
Jacobs et al. [1996]*	73
Assmann et al. [2003]*	83
Holland et al. [2003]*	27
Smethie and Jacobs [2005]	20 – 60
Horgan et al. [2011]	16

*denotes paper that reported melt rates in cm a^{-1}. Results were converted to $km^3\ a^{-1}$ using a mean RIS base area of 330,000 km^2 .

of only -0.0004 per decade, and two orders of magnitude less than the -0.03 per decade JG10 freshening of HSSW. If we assume the JG10 freshening applies to all SW within the Ross Sea, the increase in glacial melt water from the GCT after 2000 would account for only one percent of this freshening.

The AASW layer (3.08×10^4 km^3) of the Ross Sea inshore of the shelf break has a mean salinity of 34.31. A lack of discernable LAT melt water input through 2000 would preserve this salinity, however, after 2000 a consistent increase of 1.49 $km^3\ a^{-1}$ of new fresh water would result in a 2011 AASW layer salinity of 34.29. Given the AASW freshening trends from JG10 (-0.08 per decade) and a -0.07 per decade freshening of AASW in the Eastern Ross Sea [S06], glacial melt water inputs from the LAT can account for 12 – 14% of the reported freshening over the 1992 to 2011 period.

Using a 25 km x 25 km climatology of the entire Southern Ocean [*Orsi and Whitworth III*, 2005a], we can estimate the effect of melt water sources on AASW (γ^n = 27.9 kg m^{-3}) within the 1.88×10^5 km^2 Amundsen Sea (black box, Figure 3.19). From a

mean CTD profile of density within this region, the base of the AASW layer is around 400 m, thus giving an AASW volume of 7.52 x 10^4 km^3. If we assume the volumetric mean salinity of 33.99 is characteristic of 1992, consistently increasing melt water inputs from the Dotson and PIG glaciers (3.25 km^3 a^{-1}) would freshen the AASW volume to 33.96 by 2011, a -0.015 decrease per decade.

If the Amundsen Sea anomaly reaches the entrance to the Ross Sea downstream, assuming no change in the transport and entrainment rates, it would account for 30% of the observed freshening (-0.05 per decade) of AASW at 200-m in the ACoC at Cape Colbeck (Figure 3.20). Thus other marine glacial ice systems between the Amundsen and Ross Sea could be contributing unknown volumes of melt water to account for the remaining 70%. Regardless, even if this entire anomaly enters the Ross Sea, local processes would still need to account for a 0.02 – 0.03 per decade freshening.

From the PRISM historical moorings and the 2010-2011 Eastern Ross Sea project moorings, it appears our estimates of melt water transports are likely conservative because the coldest waters with the highest melt water fraction are recorded during the austral winter (May through August). Thus, assuming the volume transports do not change much throughout the year, the summer melt water transports calculated here are likely underestimates of the total melt water flux for the entire year.

Most estimates of RIS melt rates (Table 3.11) assume that melting occurs near the grounding line and at the outer edge of RIS, with active freezing in the middle. Thus basal melt rates likely do not affect the whole ice shelf [*Assmann et al.*, 2003; *Grootes and Stuiver*, 1985; *Holland et al.*, 2003; *Horgan et al.*, 2011; *Rignot and Jacobs*, 2002;

Zotikov et al., 1980]. Modeled ice shelf melting shows a relatively large area of melting at the grounding line along Sipple Coast (153°W, 81.5°S) [*Holland et al.*, 2003] near the front of the RIS. This actively melting region is aligned with the outflow path of increasing LAT melt water, and could thus be a potential source of this increase.

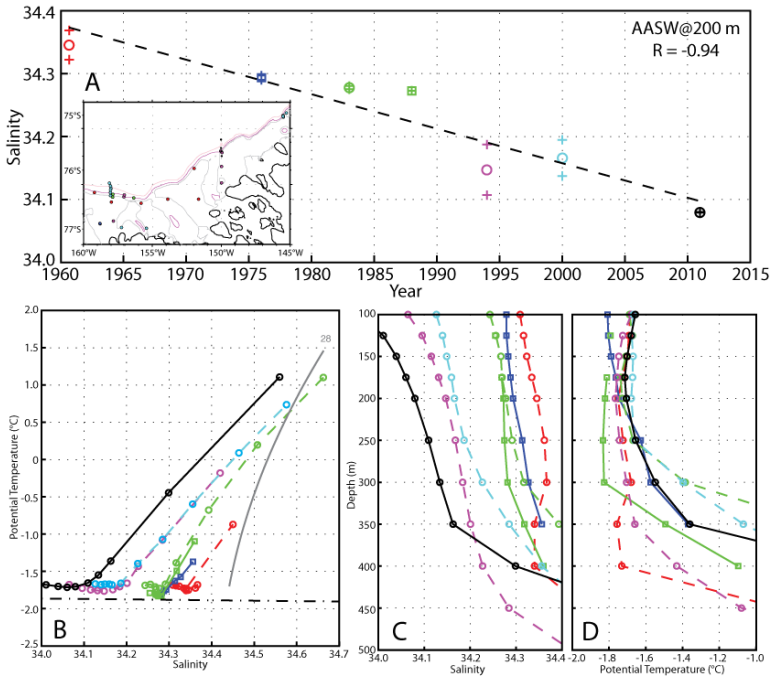

Figure 3.20: Temporal variability of inflowing AASW near Cape Colbeck at 200 m. a) Five-year mean (circles/squares) salinity at 200 m versus year with 1-standard deviation (plus) above and below and linear best-fit line shown as the dashed black line. Inset shows the station locations. b) Potential temperature versus salinity for five-year means. c) Salinity and d) potential temperature versus depth for five-year means.

CHAPTER IV

SEA ICE VARIABILITY AND EFFECTS ON ROSS SEA WATERS

Studies of sea ice coverage have provided a much greater understanding of air-sea interactions and long-term changes in polar regions since the early 1970s [*Cavalieri and Parkinson*, 2008; *Cavalieri et al.*, 1997; *Parkinson and Cavalieri*, 1989; 2002; 2008; *Parkinson et al.*, 2006; *Parkinson et al.*, 1999; *Stammerjohn et al.*, 2008; *Zwally et al.*, 2002]. In the northern hemisphere, sea ice extent is declining at a remarkable rate of 3.7 percent per decade [*Parkinson and Cavalieri*, 2008], whereas it is growing around Antarctica by one percent per decade, with the exception of the Amundsen and Bellingshausen seas where sea ice is shrinking at a rate of 5.4 percent per decade [*Cavalieri and Parkinson*, 2008]. However, in contrast to the Arctic, studies of Antarctic sea ice variability are constrained by scarce in situ observations and unreliable data derived from satellites. Available sea ice data are heavily biased by shipping routes and still not comprehensive enough to determine any long-term variability [*Worby et al.*, 2008]. Only recently are there satellites equipped with altimeters capable of measuring sea ice thickness [*Kurtz and Markus*, 2012], which still need to be ground-truthed with in situ observations.

As a seemingly unorthodox use of the National Ice Center operational ice charts, a new hemispheric high-resolution (25 km x 25 km) long-term (2000 – 2009) time series of sea ice extent, area, thickness and volume were created to gain a better understanding of Antarctic variability [*DeLiberty et al.*, 2011; *Morgan*, 2011].

Long-Term Trends

Here we take advantage of this new dataset to analyze the effect of sea ice variability on Ross Sea water masses. The time series were extended through 2011 and reanalyzed for trends.

In the Ross Sea, sea ice has gained area from 2000 to 2011 at a rate of ~20 x 10^3 km^2 a^{-1} (Table 4.1; Figure 4.1), whereas there is only a slight increase (2.58 x 10^3 km^2 a^{-1}) in the Amundsen/Bellingshausen region at about an order of magnitude slower rate. While typically lumped together, the Amundsen and Bellingshausen seas are separated in this study to investigate their regional responses. In fact, the two areas appear to be changing in almost the exact opposite sense: a decrease (-3.87 x 10^3 km^2 a^{-1}) in the Bellingshausen and increase (4.24 x 10^3 km^2 a^{-1}) in the Amundsen, i.e. increasing about five times slower than in the Ross Sea. Thus, the Bellingshausen dominates the regional decrease (130°W-60°W) reported by Cavalieri and Parkinson [2008]. Furthermore, our estimated decline in this region is consistent with the anomalous warming over the Antarctic Peninsula [*Vaughan et al.*, 2003].

Antarctic mean sea ice thickness has increased in all the three selected regions during 2000 to 2011 (Table 4.1; Figure 4.2). Furthermore the Ross and Amundsen seas show almost the same rate of increase (1.5 cm a^{-1}), whereas the Bellingshausen increase (0.45 cm a^{-1}) is nearly four times slower. The newly estimated sea ice volume has also increased in all three regions, but a remarkably larger Ross Sea rate is revealed (86.76 km^3 a^{-1}), about three times faster than in the Amundsen (25.27 km^3 a^{-1}; Figure 4.3). The odd behavior of a volume increase (3.88 km^3 a^{-1}) equal and opposite to the area decrease

for the Bellingshausen is likely due to an increase in snow accumulation [*Turner et al.*, 2005] on the ice, thus a "thickening". While these unique estimates of changing thickness and volume give us greater insight on their regionality and evolving nature, they do not necessarily reflect on variability in production rates.

Table 4.1. Rate of change for sea ice from 2000 - 2011 using the new NIC dataset.

Region	**Area** (10^3 km^2 a^{-1})	**Extent** (10^3 km^2 a^{-1})	**Thickness** (cm a^{-1})	**Volume** (km^3 a^{-1})
Ross Sea (160°E – 130°W)	19.93	19.23	1.84	86.76
Amundsen and Bellingshausen (130°W – 60°W)	2.58	1.95	1.41	25.27
Amundsen (130°W – 100°W)	4.24	4.32	1.81	19.85
Bellingshausen (100°W – 60°W)	-3.87	-4.61	0.45	3.88

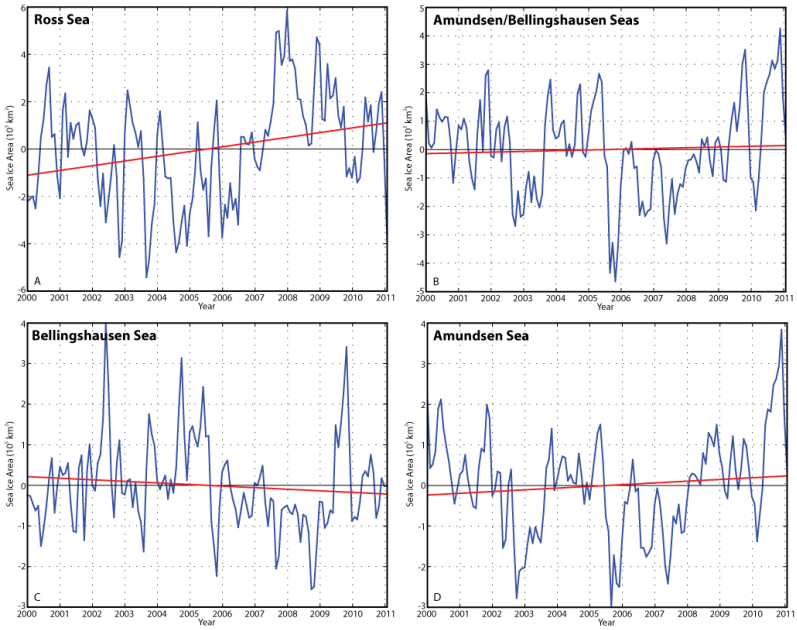

Figure 4.1: Monthly anomalies of sea ice area. Shown in blue are a) the Ross, b) Amundsen/ Bellingshausen, c) Bellingshausen and d) Amundsen seas with linear trends in red.

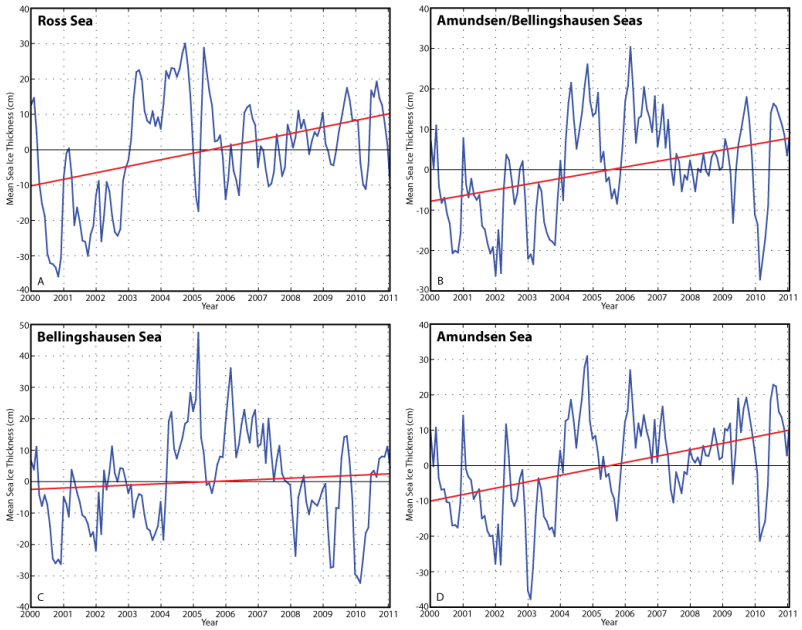

Figure 4.2: Monthly anomalies of mean sea ice thickness. Shown in blue are a) the Ross, b) Amundsen/ Bellingshausen, c) Bellingshausen and d) Amundsen seas with linear trends in red.

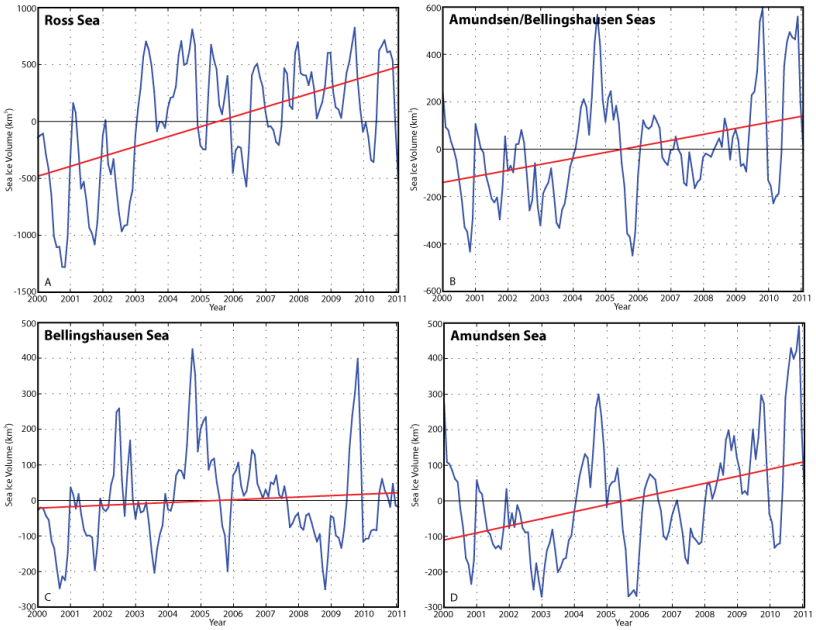

Figure 4.3: Monthly anomalies of sea ice volume. Shown in blue are a) the Ross, b) Amundsen/ Bellingshausen, c) Bellingshausen and d) Amundsen seas with linear trends in red.

Production Rates in the Ross Sea

Recent studies of sea ice production rates in the Ross Sea make assumptions about sea ice thickness [*Comiso et al.*, 2011; *Jacobs et al.*, 2002; *Martin et al.*, 2007], e.g. a constant average thickness determined from shipboard measurements [*Jeffries and Adolphs*, 1997] or derived from algorithms applied to passive microwave data [*Martin et al.*, 2007]. The latter estimated a productivity increase for the RIS Polynya of 10 km^3 a^{-1} (1992-2002), whereas independently Comiso et al. [2011]; herein Co11; estimated a rate almost twice as large. Their ~20 km^3 a^{-1} rate (1992-2008) was derived from two different calculations. Using ice-drift data, they estimated an increase of the net export of sea ice from the Ross Sea at ~30,000 km^2 a^{-1} (Figure 4.4) with a constant thickness of 0.6 m [*Jeffries and Adolphs*, 1997]; and from the analysis of the size of the RIS Polynya combined with a varying thickness derived from an algorithm. Both studies agree, however, that an increased sea-ice production will have a direct salinification effect on the local SW and suggest that the observed long-term freshening [JG10] is likely the result of incorporating freshwater anomalies from the Amundsen Sea. Making assumptions on volume and mean salinities, Co11 estimated an increase in SW salinity of 0.023 per decade, almost exactly opposite of the -0.03 per decade decrease reported by JG10.

The new thickness time series discussed in this study provides a reasonable independent production estimate after 2000. The known volumes of resident water masses from the new Ross Sea high-resolution climatology [OW09; S06] allow us to estimate the effect of sea ice production variability on the internal salinity of AASW and

SW. Using yearly net sea-ice area export data from Co11 (Figure 4.4) for 2000 – 2008 alone, renders a decrease of -16.25 km^2 a^{-1} in local sea ice area export, which for a constant ice thickness of 0.6 m yields a production decrease of -9.75 km^3 a^{-1} (green dashed line, Figure 4.5). A similar long-term trend (-9.86 km^3 a^{-1}; blue dashed line) is derived using the new yearly mean (NIC climatology) thickness values for the Ross Sea area inshore of the 700-m isobath, with the enhanced variability expected from the thickness time series. Thus a reduction in the amount of brine released into the surrounding Ross Sea water is calculated for the 2000 – 2008 period.

During sea ice formation, we assume that 79% of the salt from AASW is rejected [*Skogseth et al.*, 2004]. The volumetric (3.08×10^4 km^3) mean salinity of AASW found over the shelf is 34.31, so for every 1 km^3 of ice formed there is 3.43×10^{-2} Gt of salt left behind. Thus, AASW available to sink into the SW layer after surface cooling would be 0.17 saltier (0.22 per decade) after eight years (1992-2000) of sea ice production increasing at a rate of 20 km^3 a^{-1}. In contrast the decreasing rate calculated for after 2000 in this study would lower the AASW salinity to 34.36 by 2011, a freshening of 0.11 per decade. The overall net effect of the piece-wise trends would yield an increase in the mean salinity of 0.03 per decade from 1992 to 2011.

It is assumed in this study that all the salt rejected during freezing of AASW described above sinks into the SW layer (1.15×10^5 km^3) [OW09; S06] and is mixed uniformly. The Co11 rate estimate for 1992-2008 would increase the SW salinity unrealistically by 0.04 per decade, opposite to that of JG10. This estimate does not assume the reported a -0.08 per decade freshening reported by JG10. Accounting for this

would only slow the salinification of the SW layer by 0.0002 per decade, much less than the overall effect of the increasing sea ice production. In fact, an AASW freshening of ~20 per decade would be needed to counteract the increasing sea ice production and freshen the SW layer by the JG10 estimate. However, our estimated decrease in sea ice production of -9.86 km^3 a^{-1} during 2000-2008 would freshen the SW layer by 0.02 per decade accounting for 66% of the observed JG10 variability.

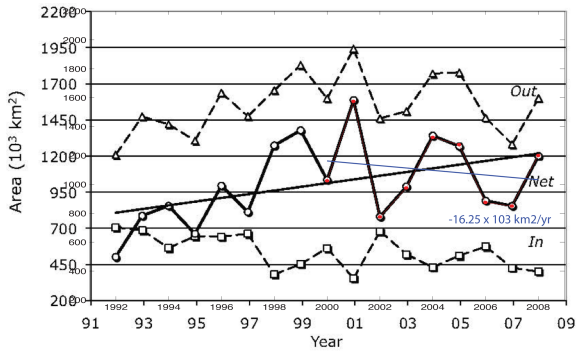

Figure 4.4: Ice area inflow, outflow, and net export for the Ross Sea winter. The blue line is the linear trend from 2000 to 2008. Figure adapted from Comiso et al. [2011].

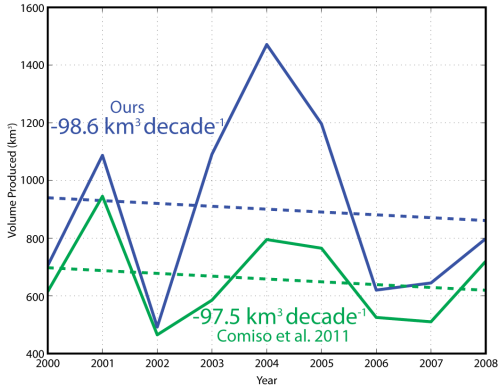

Figure 4.5: Annual volume of sea-ice production in the Ross Sea from 2000-2008. The Comiso et al. [2011] ice area export from Figure 4.4 with a mean thickness (green) and with our Ross Sea shelf winter mean thickness (blue) are shown. The blue (green) dashed line is the -98.6 (-97.5) km^3 $decade^{-1}$ linear trend.

CHAPTER V

EVOLVING MIXING RECIPES

The observed long-term changes in the characteristics of AASW, MCDW, and SW of the Ross Sea (see Chapter I) are likely to bear some effect on the properties of their water mixtures assuming isopycnal mixing near the shelf break remained the same. The new Ross Sea climatology incorporated all available bottle and CTD data spanning 1928 to 2004, therefore potential decadal variability in water mass properties was averaged out, but their steady-state volumetric mean properties and mixing ratios are calculated instead. The means at the outer shelf and slope regions of the Drygalski and Joides troughs, when compared to decadal trends reported by JG10, are representative of values from 1992 values. Therefore, for the purpose of this exercise, the new climatology represents 1992 conditions.

Salty (S = 34.79) near freezing SW (green dot, Figure 5.1a) in the western shelf break region diapycnally mixes with relatively fresher (S = 34.62) and warm (θ = -0.07°C) inflowing MCDW (blue dot) to produce MSW that is light enough to clear the local sills and replenish isopycnally the climatological newly exported AABW ($\gamma^n \approx$ 28.29 kg m^{-3}) found over the western slope (purple dot). A mixture of 80% MCDW and 20% SW would produce the regional source MSW found farther inshore at roughly the same density (cyan dot). Therefore we deduce that in 1992 the downslope sinking of newly-formed AABW in the western Ross Sea was typically representative of an 80/20 mixture of MCDW/SW.

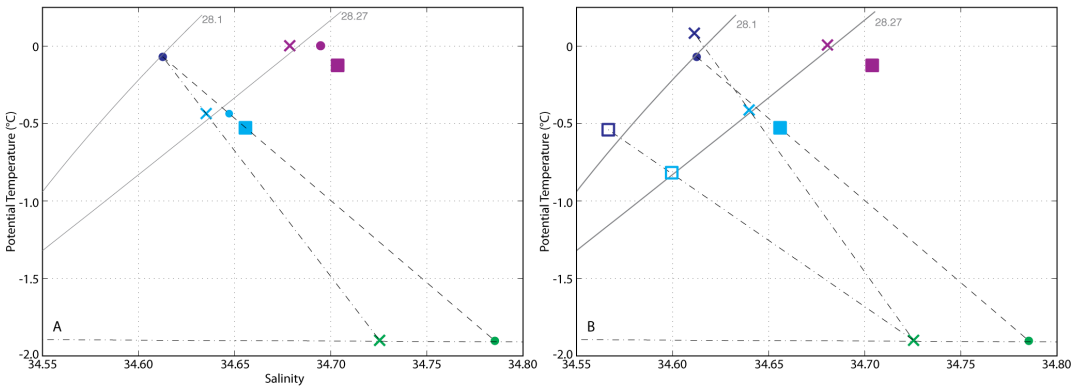

Figure 5.1: Mixing scenarios for waters at the Ross Sea shelf break. The climatological mean salinity (representative of 1992 conditions) for SW (green), MCDW (blue) and offshore AABW (purple) are shown by the colored dots. The mean AABW at Cape Adare from 1992 (2011) WOCE S4P stations is shown by the purple square (x). SW freshened by 0.06 [JG10] is indicated by the green x. a) The black dashed lines show the 1992 80/20 (75/25) MCDW/SW mixing to produce MSW with properties shown by the cyan dot (square) and the 2012 79/21 mixing to produce the cyan x. b) The 75/25 (79/21) mixing of warmer (colder and fresher) MCDW shown by the blue x (square) with SW produces MSW with properties indicated by the cyan x (square). The dash-dot line is the temperature of the surface freezing point. The grey lines show selected neutral density surfaces.

Effects of Shelf Water Variability

From the reported SW freshening (-0.03 per decade) [JG10] and no significant temperature change, its salinity would be 34.73 by 2012 (green x, Figure 5.1a). Without altering the MCDW properties the same 80/20 mixing recipe results in MSW with a neutral density of $\gamma^n \approx 28.26$ kg m^{-3} (green x). The offshore AABW showed no significant temperature trend, but a freshening of 0.008 per decade [JG10], therefore the 2012 volumetric mean salinity would be 0.016 fresher (purple x) and with the same density ($\gamma^n = 28.26$ kg m^{-3}) of the MSW in 2012. The fact that the 1992 and 2012 difference in θ-S characteristics of MSW and AABW along isopycnals are roughly the same indicates that the estimated freshening of SW is enough to account for the salinity reduction observed in the AABW outflow farther offshore.

Compared to WOCE 1992 conditions, the recent repeat CLIVAR hydrography from the S4P line (2011) shows warming of outflowing AABW off Cape Adare (purple x, Figure 5.1). Following JG10 the bottom 1000 m properties were averaged for stations at water depths greater than 2500 m. AABW properties in 1992 (purple square) were colder (θ = -0.12°C) and slightly saltier (~34.70) than the climatology value (θ = 0°C, S = 34.69), but very close to the 1992 salinity (34.70) and temperature (θ = 0.1°C) in the JG10 trend. To produce AABW with γ^n = 28.32 kg m^{-3} in 1992, the inshore MSW (cyan square) at that density would require 75% MCDW and 25% SW.

The mean AABW properties observed in 2011 are almost identical to the "freshened" climatology and at the rate reported in JG10 (-0.008 per decade). However, the corresponding MSW (cyan x) inshore would be a mixture with 4% more MCDW (79%) and less SW (21%).

Effects of MCDW Variability

In theory warmer MCDW would result from enhanced heat transport across the shelf break in response to the positive Southern Annular Mode (SAM) index during the past couple of decades [*Hall and Visbeck*, 2002]. Such a scenario is simulated by warming the 1992 MCDW by 0.15°C for 2012 conditions (blue x, Figure 5.1b), i.e. warming trend of 0.075°C per decade. The same 75/25 mixing recipe of 1990 results in a slightly lighter ($\gamma^n \approx$ 28.27 kg m^{-3}) MSW (cyan x), the same density as the AABW offshore in 2011 (purple x). Nonetheless, JG10 have shown that MCDW at the RIS front in the GCT, which varies little from at the shelf break, has freshened (-0.04 per decade) and also progressively cooled by ~ 0.5°C over a 30 year period, i.e. at -0.17°C per

decade. Thus, these trends will be used to analyze the effects of the observed waning MCDW on AABW formation. Thus, if MCDW (blue square) cooled (freshened) by -0.54°C (-0.046) twenty years later, it would be a mixture of 79% MCDW and 21% SW (green plus).

The previous exercise demonstrates that the same 79/21 (MCDW/SW) mixing product would result from multiple combinations of varying ingredients. However, the colder and fresher MCDW scenario is more consistent with the observed properties in 2011 and demands sinking SW to entrain relatively larger amounts and/or warmer CDW offshore. Entrainment of warmer CDW seems more likely as it is supported by observations: offshore of Drygalski and Joides Banks [S06], CDW increased temperature (salinity) at 0.07°C (0.0075) per decade, and new deep and bottom waters at the continental rise farther downstream (off Cape Adare) in 2011 have warmed at about the same rate since 1992.

CHAPTER VI

CROSS-SHELF TRANSPORT

Introduction

To quantify the relative influences on Ross Sea water characteristics from the observed variability in sea-ice production and glacial melt water inputs, a transect along the outer shelf (Figure 6.1) is constructed using the new high-resolution (5-km grid spacing) climatology [S06]. Property and geostrophic velocity fields are shown in Figures 6.2 and 6.3. These velocities were then balanced for volume, potential temperature, salinity and oxygen using the inverse method described in Chapter III.

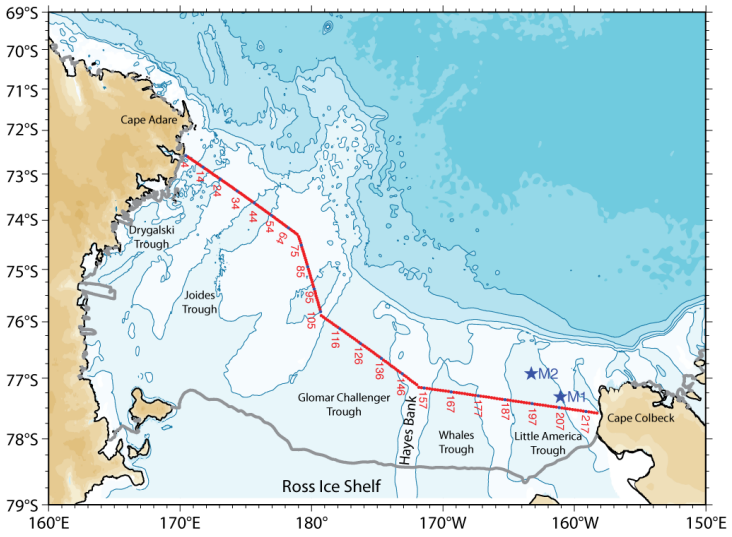

Figure 6.1: Basemap of the climatological section in the Ross Sea. The locations of the constructed transect from the high-resolution climatology (red line) and 2010-2011 eastern Ross Sea moorings (blue stars) are shown.

Layered Water Mass Structure Near the Shelf Break

The warmest MCDW inflow (Figure 6.2) is found over the Joides Trough where water warmer than -0.4°C hugs its eastern flank around 175 m, whereas the weakest is located over Hayes Bank ($\gamma^n < 28.1$ kg m^{-3}, $\theta > -1$°C). Two additional cores of MCDW with intermediate characteristics are clearly seen in the central Drygalski Trough ($\theta > -0.6$°C, $O_2 < 6.0$ ml l^{-1}) and along the eastern side of Iselin Bank ($\theta > -0.8$°C, $O_2 <$ 5.4 ml l^{-1}). Of these two cores, the relatively saltier ($S > 34.6$) and more oxygenated Drygalski MCDW indicates greater vertical mixing with outflowing SW.

Distinct varieties of MSW/SW are found in each cross-shelf trough. The saltiest ($S > 34.8$) and densest ($\gamma^n > 28.75$ kg m^{-3}) SW in the Drygalski Trough is practically blocked to the north by the local sill. Although the thin bottom layer of the Joides Trough and GCT are filled with salinities as high as 34.75, the sills also restrict their outflows. The bulk of MSW/SW outflows from these two troughs are relatively fresh ($S<34.7$), which is also present in the Drygalski within a thin layer (~100 m) above the more volumetric salty outflow from that Trough. The lowest salinity ($S < 34.6$) MSW/SW outflows are located in the Whales and LAT, although the easternmost is almost completely closed off from ventilating the deep ocean by the relatively deep (575 m) local sill.

Near Cape Colbeck, the thickest (> 400 m) most voluminous AASW is also the freshest ($S < 34$) at the sea surface. The AASW layer progressively thins and increases its salinity towards the west from $S < 34.4$ in the intermediate troughs, to 100 m thick in the Drygalski Trough with $S = 34.5$.

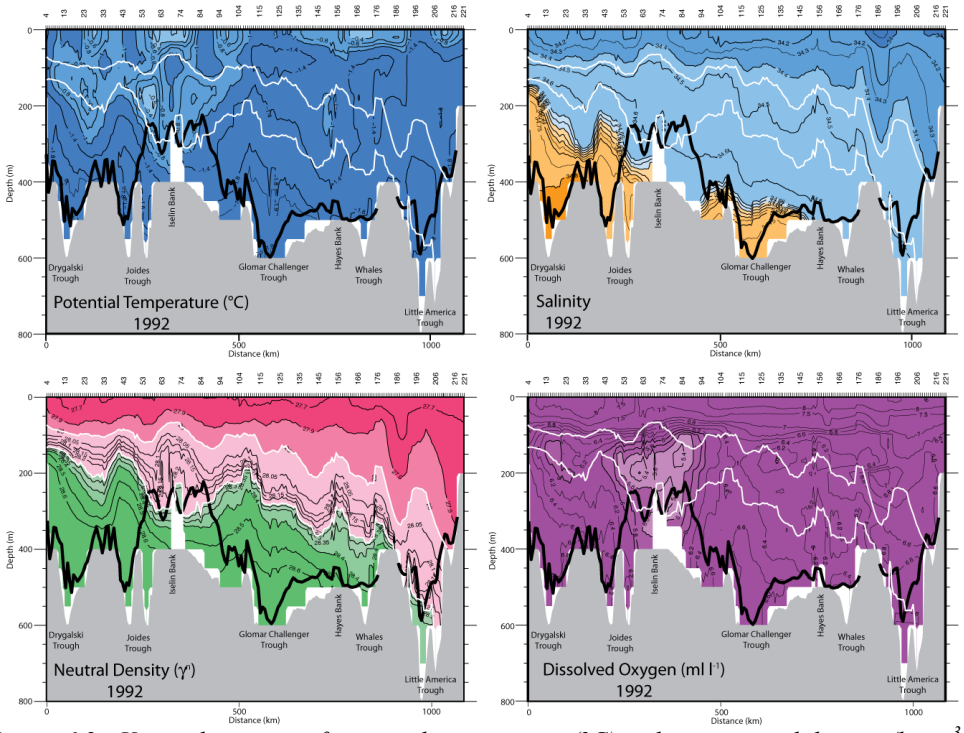

Figure 6.2: Vertical sections of potential temperature (°C), salinity, neutral density (kg m^{-3}), and dissolved oxygen (ml l^{-1}) for the Ross Sea climatological section just inshore of the shelf break. The thick black line is the approximate sill depth of each trough at the shelf break and the white lines are traces of the 28.00 kg m^{-3} and 28.27 kg m^{-3} isopycnals.

Geostrophic Currents Across the Outer Shelf

Neutral density surfaces were chosen as the level of no motion to separate warm salty inflows of MCDW from cold dense outflows of MSW/SW. In the western and central Ross Sea, the lower limit of MCDW (γ^n = 28.27 kg m^{-3}) was used from Cape Adare to grid point #185, where it runs aground on the western flank of the LAT. Farther to the east, the isopycnals are much steeper than in the rest of the section and there is little volumes of MSW/SW, thus the reference level is raised to the upper limit of MCDW (γ^n = 28.00 kg m^{-3}). The resulting baroclinic velocity field (Figure 6.3) is a highly banded estuarine flow structure, but still resolves the major known circulations:

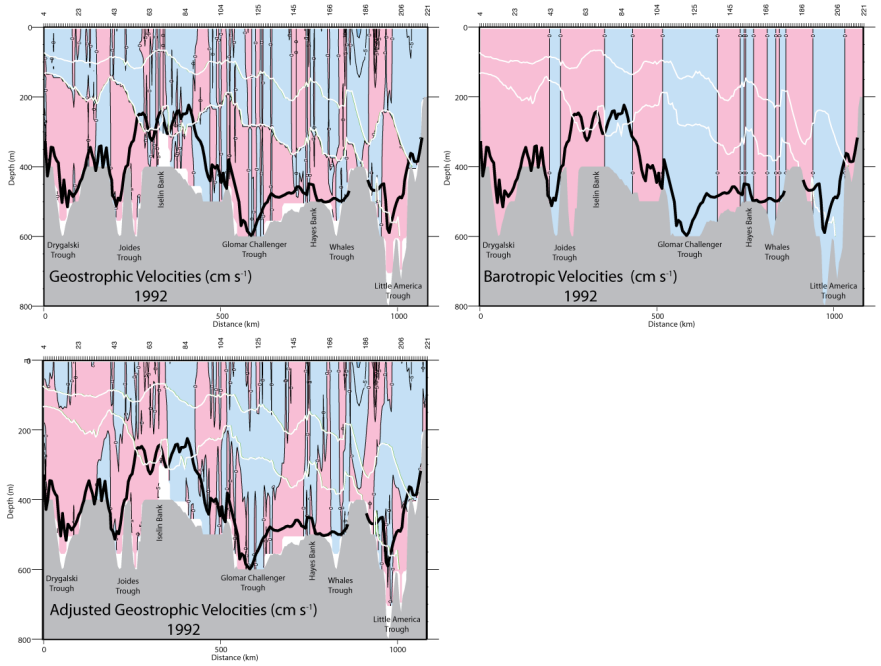

Figure 6.3: Geostrophic, barotropic, and adjusted geostrophic velocities (cm s^{-1}) for the Ross Sea climatology section. Positive (negative) velocities are shown by the pink (blue) shades. The thick black line is the approximate sill depth of each trough at the shelf break and the white lines are traces of the 28.00 kg m^{-3} and 28.27 kg m^{-3} isopycnals.

inflowing ACoC in the east, outflows of MSW/SW from the three westernmost troughs, and inflowing MCDW.

The barotropic velocity field derived from the inverse method yields a pattern with wide bands (Figure 6.3). These adjustments are very small, on average only mm s^{-1} and at most 1-2 cm s^{-1}. When added to the baroclinic velocities, the adjusted circulation pattern across this section is clearly more consistent and realistic with the distribution of property cores described above (Figure 6.3): 1) a relatively deep-reaching and broad band of strong (>5 cm s^{-1}) southward-flowing AASW is found over the eastern flank of the LAT indicating the poleward extension of the ACoC; 2) a full water column ~150 km wide inflow of MCDW over the Iselin Bank, part of which returns northward with

attenuated characteristics along the eastern flank of the Drygalski Trough; 3) a narrow and weaker inflow of MCDW over Hayes Bank; 4) Widespread outflow of MSW/SW over the Drygalski and Joides troughs; 5) more irregular banded circulations within the eastern troughs including relatively wide pockets of northward flow, in particular along the eastern flank of the LAT beneath the ACoC.

Shelf-Deep Ocean Exchange

The cumulative volume transports of the baroclinic velocity field across the outer-shelf section (dashed line, Figure 6.4a) yields a net inflow of almost -0.25 Sv (1 Sv = 10^6 m^3). However, under the assumption of negligible atmospheric exchanges within the shelf domain, the adjusted geostrophic velocity field resulting from the inverse method complies with the conservation of volume. The layered adjusted geostrophic transports are discussed next.

A net AASW inflow of 0.87 Sv (Figure 6.4b) results mainly from the prominent (80 km wide) ACoC with 0.62 Sv, and 0.25 Sv into the Whales Trough. These two inflows allow for AASW to reach the far end of the Ross Sea, and continue westward in front of the RIS where cooling and sea-ice formation transforms its characteristics. To the west of Hayes Bank a series of minor (<0.18 Sv) inflows and outflows compensate with each other.

The intermediate MCDW layer has an overall cyclonic circulation with a net poleward transport of 0.025 Sv east of Hayes Bank (Figure 6.4c), i.e. thirty-five times smaller than AASW inflow above. No net meridional transport is estimated between Cape Adare and Hayes Bank, but about 0.15 Sv flow cyclonically around the Iselin

Bank, consistent with the inflow of the oxygen-poor MCDW core along its eastern flank. Within the Whales and LAT, the sill entrapment of volumes of SW flavors vertically mix with southward-flowing MCDW to produce the low-salinity AABW exported from the LAT [*Locarnini*, 1994]. The rest of the local input of MCDW mixes vertically with AASW of the ACoC to form the lighter "non-bottom" outflow of new deep waters described in OW09, which effectively ventilates the adjacent deep ocean along the 28.20 kg m^{-3} isopycnal. Thus, by splitting the MCDW layer appropriately in the middle, i.e. at the γ^n = 28.15 kg m^{-3} following OW09, one can clearly distinguish the shallow 0.058 Sv inflow of upper MCDW (Figure 6.5) that is completely unobstructed by any major bank from Cape Adare to the Whales Bank, where the 28.15 kg m^{-3} isopycnal runs aground (Figure 6.2). The net outflow of lower MCDW (0.033 Sv), also referred to as new Antarctic Deep Water (ADW) [*Smith et al.*, 2012], and is mainly localized of the Joides (0.08 Sv) and Drygalski (0.05 Sv) troughs.

The net outflow of MSW/SW of 0.88 Sv (Figure 6.4d) from the Ross Sea is about one third of the global SW export [*Orsi et al*., [1999]. These bottom outflows directly contribute to the observed AABW layer at the foot of the continental rise off Cape Adare, which incorporates downslope entrainment of warmer ambient waters. The largest SW outflows (~150 km wide) are found across the Drygalski Trough (0.65 Sv) and the Joides Trough (0.33 Sv), whereas relatively smaller exports are located along both flanks of the GCT: 0.11 (0.08) Sv in the western (eastern) side.

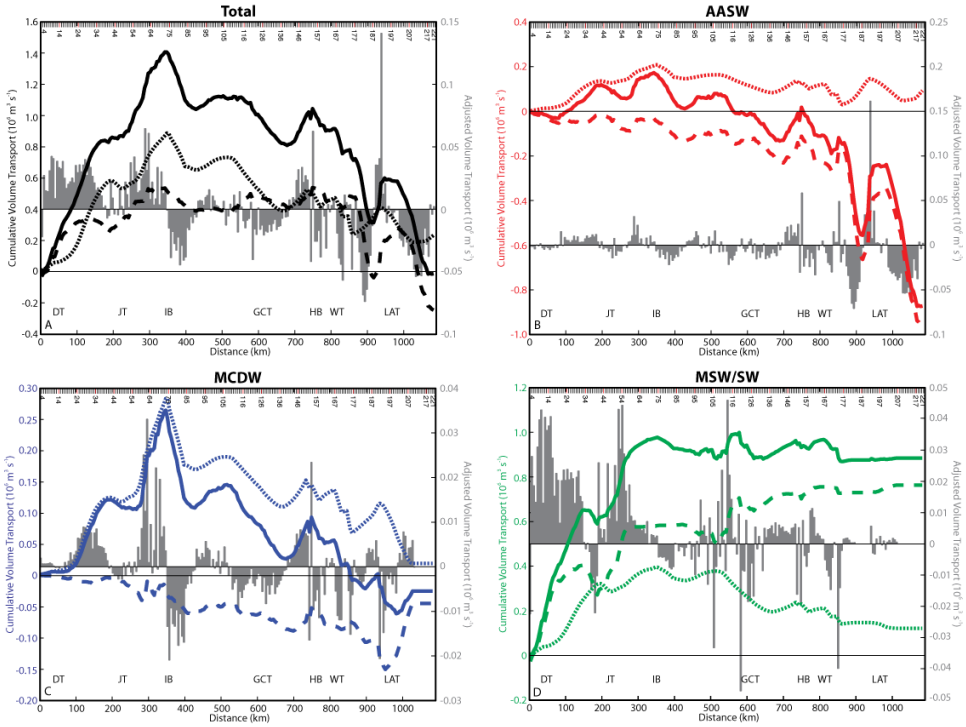

Figure 6.4: Cumulative volume transport versus distance for the Ross Sea outer shelf from Cape Adare to Cape Colbeck. The geostrophic (dashed), barotropic (dotted) and adjusted (solid) fields are shown for a) the total Ross Sea, b) the AASW layer, c) the MCDW layer, and d) the MSW/SW layer. Hash marks at the top indicate the position of each grid point. Bar plots (grey) are the associated adjusted geostrophic volume transports at each station pair. The locations of the Drygalski (DT), Joides (JT), Glomar Challenger (GCT), Whales (WT), and Little America (LAT) troughs; and Iselin (IB) and Hayes (HB) banks are labeled.

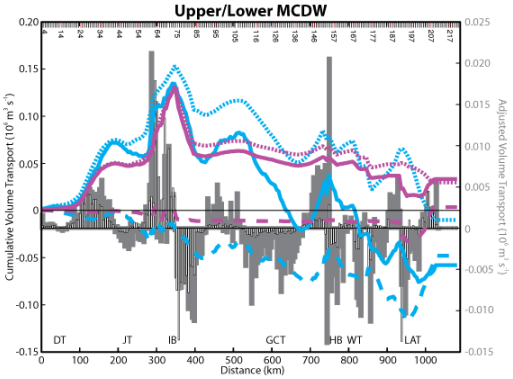

Figure 6.5: Cumulative volume transport versus distance for the upper and lower MCDW layers. The geostrophic (dashed), barotropic (dotted) and adjusted (solid) fields are shown for the upper (cyan, 28.00 kg m^{-3} < γ^n < 28.15 kg m^{-3}) and lower (purple, 28.15 kg m^{-3} < γ^n < 28.27 kg m^{-3}) layers. Dark grey (light grey with black outline) bar plots are the associated adjusted geostrophic volume transports for the inflowing (outflowing) layer at each station pair. Labels are as in Figure 6.4.

CHAPTER VII

OVERTURNING RESPONSE TO DECADAL VARIABILITY

Shelf-deep ocean exchange of MCDW across the outer shelf appears to be of lesser importance than once thought. While JG10 and S06 discuss the long-term freshening and cooling of imported MCDW, i.e. inshore of the Antarctic Slope Front, the overall effect of that variability may have a minimal impact on the decadal evolution of AASW and SW characteristics over the shelf. Because the adjusted geostrophic velocity field calculated at the outer-shelf (Figure 6.3) satisfies the conservation of volume, the net poleward imbalance of AASW (0.87 Sv) in the eastern Ross Sea must be transformed into a different water mass within the shelf interior. It is most likely that nearly all of this volume is converted into SW through winter buoyancy loss. In fact the net the southward flow of AASW entering the shelf to the east of Hayes Bank almost exactly matches the outflow of MSW/SW mostly concentrated in the western Ross Sea. This could be loosely translated as the total production rate of SW within the Ross Sea. To account for the production of 0.8 Sv of SW in 1992, the formation of over 3,000 km^3 of sea-ice would have been needed during that year's winter season. Rather than attributing this to a grossly underestimated sea ice production rate in 1992, we assume that the remaining 90 percent of AASW volume is likely converted into SW through heat loss at the sea surface.

Residence Times of Ross Sea Water Masses

Combined with the meridional volume transport at the outer shelf described above, the new high-resolution Ross Sea climatology is used to quantify the residence times of each of the main water masses found over the shelf (Table 7.1). In this study, based on the interpretation of property and flow distributions in OW09, the circulation of individual water masses within each shelf-trough is considered separately. Thus, the estimated residence time of 4.70 x 10^3 km^3 for AASW over the Whales Trough is three months, whereas for the LAT 5.95 x 10^3 km^3 it is more than double (7 months), but still under one year. In contrast, the relatively larger volume of SW (75.75 x 10^3 km^3) within the Drygalski and Joides troughs has an estimated residence time of almost 2.5 years. The less voluminous (37.25 x 10^3 km^3) SW in the GCT and Whales Trough has a much longer estimated residence time of 6 years.

Table 7.1. Regional water mass volumes, transports and residence times.

Water Mass	Region	Grid Points	Total Volume Transport (10^6 m^3 s^{-1})	Inner Volume (10^{13} m^3)	Residence Time
AASW	Whales Trough	155-185	-0.56	0.470	3 months
AASW	LAT	185 – 221	-0.32	0.595	7 months
MSW/SW	GCT/Whales	107 – 166	0.11	3.725	6 years
MSW/SW	Drygalski/Joides	4 – 71	1.00	7.575	2.4 years

Effect of Changing Sea Ice and Melt Water Production on the Ross Sea Interior

To assess the evolution of Ross Sea waters in response to the observed variability in sea ice production and glacial melt water input between 1992 and 2011 a simple three-layer box model is constructed taking advantage of the new OW09 climatology, which

closely represents the observed conditions of 1992. The progressive geostrophic velocity fields across the outer-shelf section are all adjusted to satisfy continuity of volume, and used to calculate the yearly advective transport of volume (Sv) and salt (g salt a^{-1}) within each density layer. The model is initialized for 1992 with the advective volume transports described in Chapter VI, thus the entire AASW inflow (layer 1) is assumed to convect (sink) into the MSW/SW layer (3) once the volumes removed (added) from sea-ice production (glacial melt water input) corresponding to 1992 are taken into consideration. Winter convection is triggered by buoyancy loss during surface cooling to near the freezing point and sea-ice formation. The volumetric mean salinity (Table 7.2) of each water mass layer was used to calculate the 1992 salt fluxes associated with convection, sea-ice production and glacial melt water input.

As done for the volume continuity, the advective salt transports at the outer shelf section include a minor adjustment (about 2 orders of magnitude smaller than the latter) to satisfy the observed 1992 salt budget. The mass of salt injected into the SW layer from the freezing of AASW is computed as 79% of the total amount released during sea ice formation [*Skogseth et al.*, 2004]. Although sea-ice is known to form from outcropping MCDW (layer 2) in the Terra Nova Bay Polynya [OW09], the local production rate is an order of magnitude smaller than within the large Ross Ice Shelf Polynya (grey shade, Figure 1.4) [*Martin et al.*, 2007] and therefore such contribution to the salt budget is neglected in this study. However, surface variability of MCDW to near the freezing point is required to sink (convect by increase of density) the net advective flow of 1992 into the bottom layer (MSW/SW) to satisfy overall continuity.

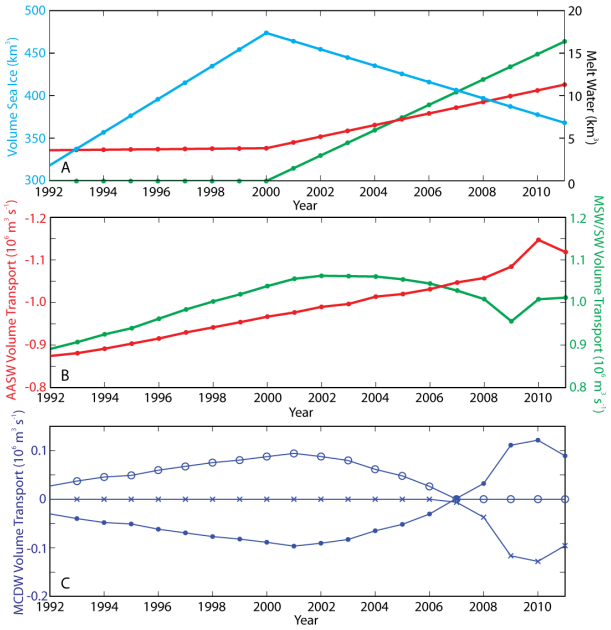

Figure 7.1: Volume transports versus year. a) Yearly freshwater volume inputs (outputs) from glacial melt water (sea-ice production) are show in red and green (cyan). b) Net yearly advective volume transport within the Ross Sea continental shelf for the AASW inflow (red) and SW outflow (green). Positive (negative) transports indicate flow into (out of) the layer. c) Yearly cumulative volume transports for MCDW advection (dots), AASW convection into layer 2 (x), and MCDW advection into the SW layer (circles). Positive (negative) transports indicate flow into (out of) the layer.

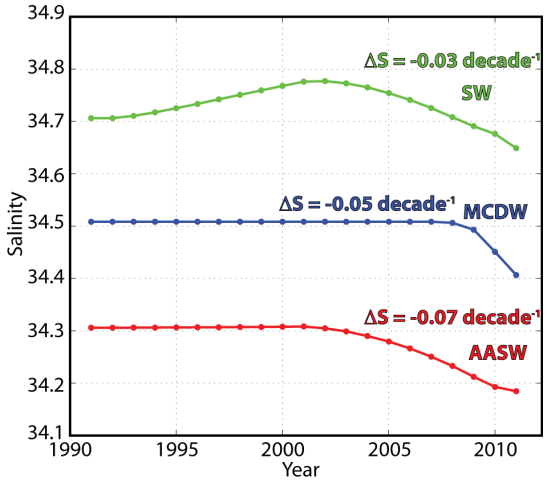

Figure 7.2: Volumetric mean salinities versus year for each Ross Sea water mass. Shown are the AASW (red), MCDW (blue) and SW (green) layers.

Table 7.2. Volumetric mean properties of water masses inshore of the outer-shelf.

Property	AASW	MCDW	SW
Salinity	34.31	34.51	34.71
Potential Temperature (°C)	-1.22	-1.35	-1.81
Neutral Density (kg m^{-3})	27.86	28.09	28.63
Depth (m)	80	200	375
Volume (10^{13} m^3)	3.08	2.69	11.48

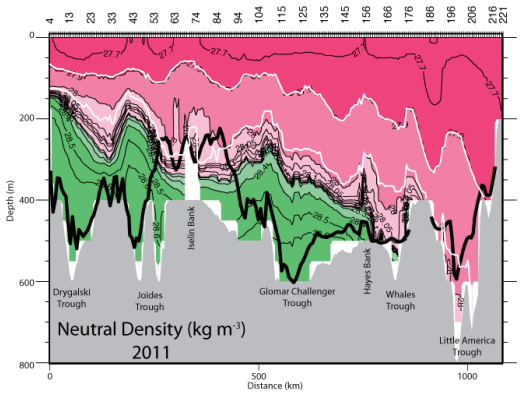

Figure 7.3: Vertical section of neutral density for 2011 for the Ross Sea climatological section just inshore of the shelf break. The thick black line is the approximate sill depth of each trough at the shelf break and the white lines are traces of the 1992 28.00 kg m^{-3} and 28.27 kg m^{-3} isopycnals.

With the initial conditions prior to 1992 estimated as described above, the model is progressed forward year by year up until 2011, each time incorporating the corresponding estimated rates of sea-ice production and glacial melt water input (Figure 7.1a) as well as the advective terms (Figure 7.1b). The yearly net salt flux imbalance for each layer is used to modify its volumetric mean salinity (Table 7.2; Figure 7.2). Consequently, the vertical salinity distribution at the outer section yields a different (recalculated) density (see the 2011 stratification in Figure 7.3) and adjusted geostrophic velocity fields, which in turn set the advective transports for the following year.

Continuity is achieved each year through the convection of AASW and, if necessary, MCDW into the bottom density layer (Figure 7.1c).

The AASW inflows and SW outflows show a slight increase in volume transport between 1992 and 2011 (Figure 7.1b): AASW by ~28% to 1.11 Sv, and SW by ~15% to 1.01 Sv. The magnitude of AASW inflows starts to exceed the SW outflows in 2006, and by 2011 was 10% larger. The transport within the MCDW layer Figure 7.2c), although one tenth in magnitude, shows a distinct evolution: steady inflow increasing from 1992 to a maximum of 0.10 Sv in 2001, followed by a more rapid decrease to near zero in 2007, and thereafter a remarkable outflow that peaked at 0.12 Sv in 2010. Even with the decline in 2011, the final outflow of MCDW is over three times larger (0.09 Sv) than the initial inflow of 1992. The reason for this switch of MCDW regimes, i.e. from inflows to outflows, is driven by the progressive addition of convective AASW volumes into the intermediate layer once AASW inflows surpassed the SW outflows by 2006.

Fresh water volume gains (inputs +) and losses (outputs -) due to the glacial met water and sea-ice production are show in Figure 7.1a. The latter volume losses are always the dominant SW contributor, and it peaked in 2000 at 473 km^3. The former inputs are larger into the SW layer up to 2000 and afterwards into the AASW layer. Although both of these volume exchanges are orders of magnitude smaller than the advective volume transports, their associated freshwater fluxes do have a significant effect on the evolution of the volumetric mean salinity of the AASW and SW layers (Figure 7.2) as shown next.

AASW maintained a relatively constant salinity of 34.31 from 1992 until 2001 due to the lack of significant amounts of freshwater inputs. The increasing amount of melt water entering the AASW layer after 2002 reduced it to 34.18 by 2011. MCDW began to freshen when the switch from net inflows to outflows occurred in 2007. The associated convection of relatively fresher AASW into this layer progressively decreases its salinity by -0.1. The mean salinity of the SW layer responds to a more complex combination of processes. From 34.71 in 1992 to 34.78 in 2002, it increased due to the steady increase in sea-ice production at a rate of ~20 km^3 a^{-1}, whereas glacial melt water inputs were minimal. After 2000, sea-ice formation decreased and glacial melt water inputs increased, which when combined with the concurrent increase in northward advective freshwater inflow, resulted in a steady freshening of SW at double the 1990s rate of increase. The longer residence time of SW (3.5 – 4 years) induces the 2-year delayed response to these changes in fluxes described above. The increase of SW outflows by 2011 is clearly inferred from the vertical section of neutral density calculated at that time (Figure 7.3). Over the Drygalski Trough, where the greatest northward transport of SW is found (Figure 6.4d), the slope of isopycnals denser than 28.27 kg m^{-3} nearly doubled since 1992 (Figure 6.2c).

This model results in a net SW freshening of -0.03 per decade between 1992 (34.71) and 2011 (34.68), which is exactly as reported by JG10 and induces a gradual increase in the drop of its top isopycnal (γ^n =28.27 kg m^{-3}) from west to east: ~25 m over the Drygalski Trough, ~75 m in the GCT, ~125 m in the Whales Trough, and completely disappeared in the LAT (~250 m drop). The modeled MCDW freshening is -0.05 per

decade from 34.51 (1992) to 34.41 (2011), a slightly larger freshening trend than reported by JG10 and S06.

Glacial melt water inputs to the AASW of the LAT are only enough to freshen that layer by -0.017 per decade, whereas JG10 reported -0.08 per decade. However, the modeled evolution with increased advective salt fluxes freshens the AASW layer to a salinity of 34.18 by 2011, i.e. a -0.064 per decade trend. This number is very close to both those of JG10 and S06 (0.07 per decade).

To test the validity of the simulated AASW salinity by 2011, a salinity time series (2010-2011) from mooring deployments at the ACoC in the LAT is inspected next. Mooring 1 is located (blue stars, Figure 6.1) just north of the outer-shelf section, and the summer (December, January, February) mean salinity recorded at 204 m is 34.19 (Figure 7.4), only 0.004 saltier than the value indicated by the model.

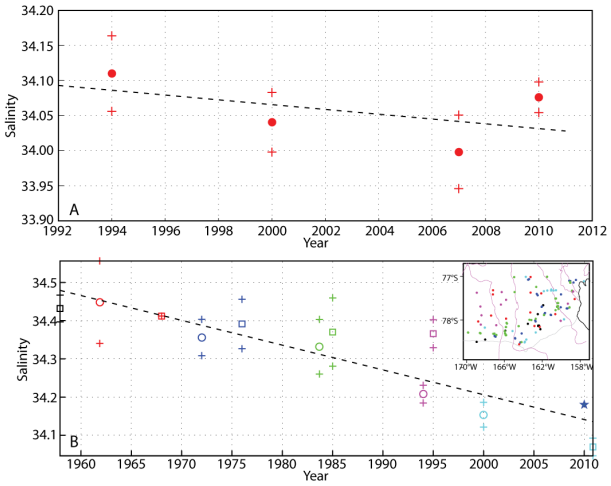

Figure 7.4: Temporal variability of AASW in the Amundsen Sea and LAT at 200 m. The a) (b) Amundsen Sea (LAT) trend spans 1994-2007 (1957-2011). The mean salinity (1-std) at 200 m indicated the by colored dots (+), whereas the linear best-fit lines are dashed. Inset shows the LAT station locations.

JG10 speculate that the main source of the freshwater anomaly required to explain the observed AASW and SW freshening is the Amundsen Sea upstream. Although sparsely sampled, data from four different years (1994, 2000, 2007, and 2010) in the southern inlet near Pine Island Bay (colored dots east of 120°W, Figure 3.19) are used compute mean profiles for each year. AASW was inspected at its mid-level (200 m; Figure 7.4) and a mean decreasing salinity trend of decrease at -0.039 per decade was calculated. The increasing glacial melt water input to AASW from the PIG and the Dotson Glacier calculated in Chapter III is enough to freshen the selected volume by -0.015 per decade, i.e. less than half of the observed salinity decrease. It is plausible that the ongoing interior freshening of the Amundsen Sea could in turn increase the adjusted fluxes like modeled here for the Ross Sea, and thus account for the missing additional (-0.025 per decade) freshening. If the measured signal were carried downstream it would likely be detected at the eastern entrance to the Ross Sea. However, near 150°W (Figure 3.20b), the observed freshening at 200-m has on average been -0.05 fresher per decade since the early 1960s, i.e. at a more rapid pace than in the Amundsen Sea. Therefore, the poorly-sampled and intricate system of glaciers and ice shelves found between the Amundsen and Ross seas may be the sources of unaccounted freshwater anomalies.

Nonetheless, for the same period (1957 – 2011) an even faster AASW freshening pace (-0.065 per decade) is observed at 200 m along the ACoC (Figure 7.4b). Therefore, the modeled evolution of both AASW and SW presented in this study agree remarkably well with the available observations in the Ross Sea: they do not rely on freshwater

anomalies originating farther upstream, but instead are entirely accounted for by local processes.

CHAPTER VIII

SUMMARY AND CONCLUSIONS

Only two hydrographic WOCE lines in the southern Pacific Ocean have been reoccupied to date as a part of CLIVAR's Repeat Hydrography Program, along 150°W (1992 and 2005) and 103°W (1994 and 2008). Antarctic Bottom Water of Ross Sea origin reaching these two lines is warmer ($\Delta\theta \approx 0.02°C – 0.035°C$) and slightly fresher ($\Delta S \approx 0.001 – 0.002$) than measured about 14 years earlier. Although seemingly miniscule, this warming is enough to cause an extensive aerial retreat and thinning of the bottom water layer colder than 0°C. What in 1994 was a 300-m thick layer at 103°W has completely disappeared by 2008. However, relatively warmer isotherms found immediately above ($\theta >= 0.1°C$) showed no vertical displacement, which indicates that the abyssal layer is replenished by the sinking of about the same volume but with slightly warmer characteristics.

Within the Amundsen Sea shelf regime, Antarctic Surface Water at 200 m has freshened by -0.03 per decade (1994 – 2007). Half of this freshening is the result of increased glacial melt water outflows (1994 – 2007) from the PIG (17.7 km^3 per decade) and Dotson Glacier (14.8 km^3 per decade). Over the narrower continental shelf regime found farther downstream, specifically along 150°W and inshore of the 1000-m isobath, the temperature minimum of AASW (200 m) has freshened by -0.05 per decade between 1961 and 2011. Therefore unknown volumes of melt water contributed by marine glacial

systems located between the Amundsen and Ross seas, e.g. the Sulzberger Ice Shelf, could contribute to account for the additional salinity decline of -0.02 per decade.

Five synoptic sections (1976 – 2007) located in front of the RIS show an increase in local glacial melt water export. In the GCT, melt water inputs have increased by 1.3 km^3 per decade, and at a more rapid pace (6.8 km^3 per decade) after 2000. Such large freshwater volume contribution is apparently not adequate to explain the observed decrease in the salinity of Ross Sea SW, i.e. it only accounts for 0.0004 per decade. The LAT was void of any glacial melt water inputs until 1994, and then remained nearly constant (~4.4 km^3 per decade) up to 2000. Similar to the GCT melt water contributions, LAT inputs drastically increased to 14.9 km^3 per decade after 2000. Although seemingly small, this increase in melt water input could freshen the local AASW by 0.017 per decade.

After a steady ~20 year (1978-2000) strengthening of the Ross Sea Polynya, its productivity trends switched from a rise (200 km^3 per decade) to a decline (-98.6 km^3 per decade) causing the estimated -0.02 per decade freshening of the SW layer.

The 1992 composition of modified SW is a mixing product of 75% MCDW and 25% SW. After the reported -0.03 per decade SW freshening and MCDW waning ($\Delta\theta$ = -0.28°C per decade, ΔS = -0.024 per decade) [JG10], MSW in 2011 consists of 4% more (less) MCDW (SW). As MSW escapes the Ross Sea sills, it progressively entrains relatively warmer CDW (0.07°C per decade) as it flows along the deep western boundary current off Cape Adare. Here, the warming (0.063 per decade) and freshening (-0.008 per decade) of new Ross Sea AABW is clearly evident in the available

hydrographic data. Thus, the evolving properties of outflowing AABW with origins in the Ross Sea are due to the local freshening of SW and warming of offshore CDW.

In 1992 the southward-flowing AASW (0.87 Sv) at the outer shelf of the eastern Ross Sea is nearly balanced by the northward-flowing MSW/SW (0.88 Sv) at the western troughs. With a residence time of approximately one year, and as a result of winter buoyancy loss, AASW sinks to the SW layer at a rate of 0.8 Sv. Intermediate MCDW cross-slope inflows are an order of magnitude smaller (0.02 Sv), and therefore play a lesser role in the overturning of the Ross Sea. However when subdivided into upper inflowing ($\gamma^n < 28.15$ kg m^{-3}) and lower outflowing components, MCDW contributes 0.03 Sv of newly ventilated waters to the deep ocean.

Sea-ice formation and glacial melt water inputs alone are not enough to explain the observed variability of Ross Sea waters. An often-neglected effect of freshwater anomalies is the induced changes in advective fluxes. Thus the response to the gradual internal adjustment of the density field is tested for the 1992-2011 period using a simple three-layer box model. During this period, inflowing AASW steadily increased by 28% to 1.11 Sv, while SW outflows increased at a slightly slower rate (15%) to 1.01 Sv by 2011. Initially the net volume transport of MCDW was southward, until it peaked in 2001 (0.10 Sv), rapidly decreased to near zero near 2007, and became a predominant outflow of 0.09 Sv by 2011.

The changing volume transports in conjunction with freshwater fluxes significantly change the volumetric mean salinities of the Ross Sea. AASW maintained a nearly constant salinity (34.31) from 1992 to 2002, when the effect of increasing glacial

melt water inputs progressively freshened it to 34.18: a net decrease of -0.07 per decade. The underlying MCDW salinity (34.51) remained unchanged until 2007, when its circulation pattern switched. Since 2007 the net outflow of new MCDW is replenished by the sinking of AASW, which induces a freshening of -0.05 per decade. SW salinity (34.71) increased from 1992 to 2002 (34.78), consistent with progressively larger sea-ice productivity. A subsequent decline in sea-ice formation rates combined with a rise in glacial melt water inputs freshened the SW to 34.68 by 2011: a net freshening of -0.03 per decade.

The estimated Ross Sea response to the evolving local freshwater fluxes produces distinct freshening trends in all the water masses, which are almost of the same magnitude as those reported in [JG10] and here, i.e. AASW freshening by -0.065 per decade in the LAT. These trends do not require any additional freshwater source from the Amundsen Sea. Although relatively fresher types of MSW/SW are currently produced in the Ross Sea, there is no apparent slow down in the export of new deep and bottom waters supplying the lower limb of the Meridional Overturning Circulation.

REFERENCES

Aoki, S., N. L. Bindoff, and J. A. Church (2005a), Interdecadal water mass changes in the Southern Ocean between 30°E and 160°E, *Geophysical Research Letters*, *32*(7), 1-4.

Aoki, S., S. R. Rintoul, S. Ushio, S. Watanabe, and N. L. Bindoff (2005b), Freshening of the Adelie Land Bottom Water near 140°E, *Geophysical Research Letters*, *32*(23), 1-5.

Arrigo, K. R., and G. L. van Dijken (2003), Phytoplankton dynamics within 37 Antarctic coastal polynya systems, *Journal of Geophysical Research-Oceans*, *108*, 1-18.

Assmann, K., H. H. Hellmer, and A. Beckmann (2003), Seasonal variation in circulation and water mass distribution on the Ross Sea continental shelf, *Antarct Sci*, *15*(1), 3-11.

Budillon, G., S. G. Cordero, and E. Salusti (2002), On the dense water spreading off the Ross Sea shelf (Southern Ocean), *Journal of Marine Systems*, *35*(3-4), 207-227.

Callahan, J. E. (1972), The structure and circulation of deep water in the Antarctic, *Deep-Sea Research*, *19*(8), 563-575.

Carmack, E. C. (1977), Water characteristics of the Southern Ocean south of the polar front, in *A Voyage of Discovery: George Deacon 70th Anniversary*, edited by M. Angel, pp. 15-41, Pergamon, Oxford.

Carmack, E. C., and P. D. Killworth (1978), Formation and interleaving of abyssal water masses off Wilkes Land, Antarctica, *Deep-Sea Research*, *25*(4), 357-369.

Cavalieri, D. J., and C. L. Parkinson (2008), Antarctic sea ice variability and trends, 1979-2006, *Journal of Geophysical Research-Oceans*, *113*, 1-19.

Cavalieri, D. J., P. Gloersen, C. L. Parkinson, J. C. Comiso, and H. J. Zwally (1997), Observed hemispheric asymmetry in global sea ice changes, *Science*, *278*(5340), 1104-1106.

Clough, J. W., and B. L. Hansen (1979), The Ross Ice Shelf Project, *Science*, *203*, 433-434.

Comiso, J. C., R. Kwok, S. Martin, and A. L. Gordon (2011), Variability and trends in the sea ice extent and ice production in the Ross Sea, *Journal of Geophysical Research-Oceans*, *116*, 1-19.

Deacon, G. E. R. (1937), The hydrology of the Southern Ocean, *Discovery Report*, *15*, 3-122.

Deacon, G. E. R. (1984), *The Antarctic circumpolar ocean*, 180 pp., Cambridge University, Cambridge.

DeLiberty, T. L., C. A. Geiger, S. F. Ackley, A. P. Worby, and M. L. Van Woert (2011), Estimating the annual cycle of sea-ice thickness and volume in the Ross Sea, *Deep-Sea Research Part II-Topical Studies in Oceanography*, *58*(9-10), 1250-1260.

Dinniman, M. S., J. M. Klinck, and W. O. Smith (2003), Cross-shelf exchange in a model of the Ross Sea circulation and biogeochemistry, *Deep-Sea Research Part II-Topical Studies in Oceanography*, *50*(22-26), 3103-3120.

Foster, T. D. (1995), Abyssal water mass formation off the eastern Wilkes Land coast of Antarctica, *Deep-Sea Research Part I*, *42*(4), 501-522.

Foster, T. D., and E. C. Carmack (1976), Frontal zone mixing and Antarctic Bottom Water formation in southern Weddell Sea, *Deep-Sea Research*, *23*(4), 301-317.

Gade, H. G. (1979), Melting of ice in sea water: a primitive model with application to the Antarctic ice shelf and icebergs, *Journal of Physical Oceanography*, *9*(1), 189-198.

Gill, A. E. (1973), Circulation and bottom water production in the Weddell Sea, *Deep-Sea Research*, *20*(2), 111-140.

Gille, S. T. (2002), Warming of the Southern Ocean since the 1950s, *Science*, *295*(5558), 1275-1277.

Gordon, A. L., and P. Tchernia (1972), Waters off the continental margin off Adelie Coast, Antarctica, in *Antarctic Oceanology II: The Australian-New Zealand sector*, edited by D. E. Hayes, pp. 59-69, American Geophysical Union, Washington, D.C.

Grootes, P. M., and M. Stuiver (1985), Land-ice/sea-ice transition in the Ross Ice Shelf at J-9, Antarctica, *Antarctic Journal of the United States*, *20*, 66-68.

Hall, A., and M. Visbeck (2002), Synchronous variability in the Southern Hemisphere atmosphere, sea ice, and ocean resulting from the Annular Mode, *Journal of Climate*, *15*(21), 3043-3057.

Hellmer, H. H., and S. S. Jacobs (1994), Temporal changes in shelf water of the southern Ross Sea, *Antarctic Journal*, *29*, 123-124.

Hellmer, H. H., and S. S. Jacobs (1995), Seasonal circulation under the eastern Ross Ice Shelf, Antarctica, *Journal of Geophysical Research-Oceans*, *100*, 10873-10885.

Hellmer, H. H., S. S. Jacobs, and A. Jenkins (1998), Oceanic erosion of an Antarctic glacier, in *Ocean, Ice, and Atmosphere: Interactions at the Antarctic Continental Margin*, edited by S. S. Jacobs and R. F. Weiss, pp. 83-99, American Geophysical Union, Washington, D.C.

Holland, D. M., S. S. Jacobs, and A. Jenkins (2003), Modelling the ocean circulation beneath the Ross Ice Shelf, *Antarct Sci*, *15*(1), 13-23.

Horgan, H. J., R. T. Walker, S. Anandakrishnan, and R. B. Alley (2011), Surface elevation changes at the front of the Ross Ice Shelf: implications for basal melting, *Journal of Geophysical Research-Oceans*, *116*, 1-12.

Jacobs, S. (2006), Observations of change in the Southern Ocean, *Philosophical Transactions of the Royal Society*, *364*(1844), 1657-1681.

Jacobs, S. S. (1989), Marine controls on modern sedimentation on the Antarctic continental shelf, *Marine Geology*, *85*(2-4), 121-153.

Jacobs, S. S., and C. F. Giulivi (1998), Interannual ocean and sea ice variability in the Ross Sea, in *Ocean, Ice, and Atmosphere: Interactions at the Antarctic Continental Margin*, edited by S. S. Jacobs and R. F. Weiss, pp. 135-150, American Geophysical Union, Washington, D.C.

Jacobs, S. S., and C. F. Giulivi (2010), Large multidecadal salinity trends near the Pacific-Antarctic continental margin, *Journal of Climate*, *23*, 4508-4524.

Jacobs, S. S., A. F. Amos, and P. M. Bruchhau (1970), Ross Sea oceanography and Antarctic Bottom Water formation, *Deep-Sea Research*, *17*(6), 935-962.

Jacobs, S. S., A. L. Gordon, and J. L. Ardai (1979), Circulation and melting beneath the Ross Ice Shelf, *Science*, *203*(4379), 439-443.

Jacobs, S. S., H. H. Hellmer, and A. Jenkins (1996), Antarctic ice sheet melting in the southeast Pacific, *Geophysical Research Letters*, *23*(9), 957-960.

Jacobs, S. S., C. F. Giulivi, and P. A. Mele (2002), Freshening of the Ross Sea during the late 20th century, *Science*, *297*(5580), 386-389.

Jacobs, S. S., A. Jenkins, C. F. Giulivi, and P. Dutrieux (2011), Stronger ocean circulation and increased melting under Pine Island Glacier ice shelf, *Nature Geoscience*, *4*(8), 519-523.

Jacobs, S. S., H. H. Helmer, C. S. M. Doake, A. Jenkins, and R. M. Frolich (1992), Melting of ice shelves and the mass balance of Antarctica, *Journal of Glaciology*, *38*(130), 375-387.

Jeffries, M. O., and U. Adolphs (1997), Early winter ice and snow thickness distribution, ice structure and development of the western Ross Sea pack ice between the ice edge and the Ross Ice Shelf, *Antarct Sci*, *9*(2), 188-200.

Jenkins, A. (1999), The impact of melting ice on ocean waters, *Journal of Physical Oceanography*, *29*(9), 2370-2381.

Jenkins, A., and S. Jacobs (2008), Circulation and melting beneath George VI Ice Shelf, Antarctica, *Journal of Geophysical Research-Oceans*, *113*(C4), 1-18.

Johnson, G. C., and A. H. Orsi (1997), Southwest Pacific Ocean water-mass changes between 1968/69 and 1990/91, *Journal of Climate*, *10*(2), 306-316.

Johnson, G. C., and S. C. Doney (2006), Recent western South Atlantic bottom water warming, *Geophysical Research Letters*, *33*(14), 1-5.

Johnson, G. C., P. E. Robbins, and G. E. Hufford (2001), Systematic adjustments of hydrographic sections for internal consistency, *J Atmos Ocean Tech*, *18*(7), 1234-1244.

Johnson, G. C., S. G. Purkey, and J. L. Bullister (2008), Warming and freshening in the abyssal southeastern Indian Ocean, *Journal of Climate*, *21*(20), 5351-5363.

Johnson, G. C., S. Mecking, B. M. Sloyan, and S. E. Wijffels (2007), Recent bottom water warming in the Pacific Ocean, *Journal of Climate*, *20*(21), 5365-5375.

Kawano, T., M. Aoyama, T. Joyce, H. Uchida, Y. Takatsuki, and M. Fukasawa (2006), The latest batch-to-batch difference table of standard seawater and its application to the WOCE onetime sections, *Journal of Oceanography*, *62*(6), 777-792.

Kurtz, N. T., and T. Markus (2012), Satellite observations of Antarctic sea ice thickness and volume, *Journal of Geophysical Research-Oceans*, *117*, 1-9.

Locarnini, R. A. (1994), Water masses and circulation in the Ross Gyre and environs, Ph.D. Thesis, Texas A&M University, College Station.

Loose, B., P. Schlosser, W. M. Smethie, and S. Jacobs (2009), An optimized estimate of glacial melt from the Ross Ice Shelf using noble gases, stable isotopes, and CFC transient tracers, *Journal of Geophysical Research-Oceans*, *114*, 1-15.

Lusquinos, A. (1963), Extreme temperatures in the Weddell Sea, *Arbok For Universitetet I Bergen: Mat.-Naturv. Serie*, *23*, 1-19.

Martin, S., R. S. Drucker, and R. Kwok (2007), The areas and ice production of the western and central Ross Sea polynyas, 1992-2002, and their relation to the B-15 and C-19 iceberg events of 2000 and 2002, *Journal of Marine Systems*, *68*(1-2), 201-214.

Morgan, B. P. (2011), Analysis of Antarctic sea ice thickness: a newly created database for 2000 - 2009, M.S. Thesis, Texas A&M University, College Station.

Newsom, K., L. Francavillese, and J. Tierney (1965), Oceanography in Operation Deep Freeze 62, 1961-1962.*Rep.*, US Naval Oceanographic Office, Marine Geophysical Investigations, Washington, D.C.

Orsi, A. H. (2010), Recycling bottom waters, *Nature Geoscience*, *3*(5), 307-309.

Orsi, A. H., and T. Whitworth III (2005a), WOCE Southern Ocean Database (http://woceatlas.tamu.edu).

Orsi, A. H., and T. Whitworth III (2005b), *Hydrographic Atlas of the World Ocean Circulation Experiment (WOCE). Volume 1: Southern Ocean*, International WOCE Project Office, Southhampton, U.K.

Orsi, A. H., and C. L. Wiederwohl (2009), A recount of Ross Sea waters, *Deep-Sea Research Part I*, *56*(13-14), 778-795.

Orsi, A. H., T. Whitworth, and W. D. Nowlin (1995), On the meridional extent and fronts of the Antarctic Circumpolar Current, *Deep-Sea Research Part I*, *42*(5), 641-673.

Orsi, A. H., G. C. Johnson, and J. L. Bullister (1999), Circulation, mixing, and production of Antarctic Bottom Water, *Progress in Oceanography*, *43*(1), 55-109.

Ozaki, H., H. Obata, M. Naganobu, and T. Gamo (2009), Long-term bottom water warming in the north Ross Sea, *Journal of Oceanography*, *65*(2), 235-244.

Parkinson, C. L., and D. J. Cavalieri (1989), Arctic sea ice 1973-1987: seasonal, regional, and interannual variability, *Journal of Geophysical Research-Oceans*, *94*, 14499-14523.

Parkinson, C. L., and D. J. Cavalieri (2002), A 21 year record of Arctic sea-ice extents and their regional, seasonal and monthly variability and trends, *Ann Glaciol*, *34*, 441-446.

Parkinson, C. L., and D. J. Cavalieri (2008), Arctic sea ice variability and trends, 1979-2006, *Journal of Geophysical Research-Oceans*, *113*, 1-28.

Parkinson, C. L., K. Y. Vinnikov, and D. J. Cavalieri (2006), Evaluation of the simulation of the annual cycle of Arctic and Antarctic sea ice coverages by 11 major global climate models, *Journal of Geophysical Research-Oceans*, *111*, 1-14.

Parkinson, C. L., D. J. Cavalieri, P. Gloersen, H. J. Zwally, and J. C. Comiso (1999), Arctic sea ice extents, areas, and trends, 1978-1996, *Journal of Geophysical Research-Oceans*, *104*, 20837-20856.

Pillsbury, R. D., and S. S. Jacobs (1985), Preliminary observations from long-term current meter moorings near the Ross Ice Shelf, Antarctica, in *Oceanology of the Antarctic Continental Shelf*, edited by S. S. Jacobs, pp. 87-107, American Geophysical Union, Washington, DC.

Purkey, S. G., and G. C. Johnson (2010), Warming of global abyssal and deep Southern Ocean waters between the 1990s and 2000s: contributions to global heat and sea level rise budgets, *Journal of Climate*, *23*, 6336-6351.

Rignot, E., and S. S. Jacobs (2002), Rapid bottom melting widespread near Antarctic ice sheet grounding lines, *Science*, *296*(5575), 2020-2023.

Rignot, E., J. L. Bamber, M. R. Van Den Broeke, C. Davis, Y. H. Li, W. J. Van De Berg, and E. Van Meijgaard (2008), Recent Antarctic ice mass loss from radar interferometry and regional climate modelling, *Nature Geoscience*, *1*(2), 106-110.

Rintoul, S. R. (1998), On the origin and influence of Adelie Land Bottom Water, in *Ocean, Ice and Atmosphere: Interactions at the Antarctic Continental Margin*, edited by S. S. Jacobs and R. F. Weiss, pp. 151-171, American Geophysical Union, Washington, DC.

Rintoul, S. R. (2007), Rapid freshening of Antarctic Bottom Water formed in the Indian and Pacific oceans, *Geophysical Research Letters*, *34*(6), 1-5.

Robertson, R., M. Visbeck, A. L. Gordon, and E. Fahrbach (2002), Long-term temperature trends in the deep waters of the Weddell Sea, *Deep-Sea Research Part II-Topical Studies in Oceanography*, *49*(21), 4791-4806.

Shabtaie, S., and C. R. Bentley (1987), West Antarctic ice streams draining into the Ross Ice Shelf: configuration and mass balance, *J Geophys Res-Solid*, *92*(B2), 1311-1336.

Sievers, H. A., and W. D. Nowlin (1984), The stratification and water masses at Drake Passage, *Journal of Geophysical Research-Oceans*, *89*, 489-514.

Skogseth, R., P. M. Haugan, and J. Haarpaintner (2004), Ice and brine production in Storfjorden from four winters of satellite and in situ observations and modeling, *Journal of Geophysical Research-Oceans*, *109*, 1-15.

Smethie, W. M., and S. S. Jacobs (2005), Circulation and melting under the Ross Ice Shelf: estimates from evolving CFC, salinity and temperature fields in the Ross Sea, *Deep-Sea Research Part I-Oceanographic Research Papers*, *52*(6), 959-978.

Smith, W. O., P. N. Sedwick, K. R. Arrigo, D. G. Ainley, and A. H. Orsi (2012), The Ross Sea in a sea of change, *Oceanography*, *25*(3), 90-103.

Stammerjohn, S. E., D. G. Martinson, R. C. Smith, X. Yuan, and D. Rind (2008), Trends in Antarctic annual sea ice retreat and advance and their relation to El Nino-Southern Oscillation and Southern Annular Mode variability, *Journal of Geophysical Research-Oceans*, *113*, 1-20.

Stover, C. L. (2006), A new account of Ross Sea waters: characteristics, volumetrics, and variability, M.S. Thesis, Texas A&M University, College Station.

Sverdrup, H. U. (1940), Hydrology, Section 2, Discussion, in *Reports of the B.A.N.Z. Antarctic Research Expedition 1921-1931, Series A2, Oceanography, Part 2, Section 2*, edited, pp. 88-126.

Trumbore, S. E., S. S. Jacobs, and W. M. Smethie (1991), Chlorofluorocarbon evidence for rapid ventilation of the Ross Sea, *Deep-Sea Research Part I*, *38*(7), 845-870.

Turner, J., T. Lachlan-Cope, S. Colwell, and G. J. Marshall (2005), A positive trend in western Antarctic Peninsula precipitation over the last 50 years reflecting regional and Antarctic-wide atmospheric circulation changes, *Ann Glaciol-Ser*, *41*, 85-91.

Vaughan, D. G., G. J. Marshall, W. M. Connolley, C. Parkinson, R. Mulvaney, D. A. Hodgson, J. C. King, C. J. Pudsey, and J. Turner (2003), Recent rapid regional climate warming on the Antarctic Peninsula, *Climatic Change*, *60*(3), 243-274.

Wahlin, A. K., X. Yuan, G. Bjork, and C. Nohr (2010), Inflow of warm Circumpolar Deep Water in the central Amundsen shelf, *Journal of Physical Oceanography*, *40*(6), 1427-1434.

Whitworth, T., and W. D. Nowlin (1987), Water masses and currents of the Southern Ocean at the Greenwich Meridian, *Journal of Geophysical Research-Oceans*, *92*, 6462-6476.

Whitworth, T., A. H. Orsi, S.-J. Kim, and W. D. Nowlin (1998), Water masses and mixing near the Antarctic Slope Front, in *Ocean, Ice, and Atmosphere: Interactions at the Antarctic Continental Margin*, edited by S. S. Jacobs and R. F. Weiss, pp. 1-27, American Geophysical Union, Washington, D.C.

Williams, A., S. Bacon, and S. Cunningham (2006), Variability of the Lower Circumpolar Deep Water in Drake Passage 1926-2004, *Geophysical Research Letters*, *33*(3), 1-5.

Worby, A. P., C. A. Geiger, M. J. Paget, M. L. Van Woert, S. F. Ackley, and T. L. DeLiberty (2008), Thickness distribution of Antarctic sea ice, *Journal of Geophysical Research-Oceans*, *113*, 1-14.

Worthington, L. V. (1981), The water masses of the World Ocean: some results from a fine-scale census, in *Evolution of Physical Oceanography*, edited by B. A. Warren and C. Wunsch, pp. 44-69, MIT Press, Cambridge.

Wunsch, C. (1978), North Atlantic general circulation west of 50°W determined by inverse methods, *Rev Geophys*, *16*(4), 583-620.

Wust, G. (1935), Schichtung und Zirkulation des Atlanticschen Ozens, Die Stratosphare., *Wissenschaftliche Ergenbinsse der Deutschen Atlanticschen Expediton auf dem Forschungs und Vermessungsschiff "Meteor"*, *6*(1), 99-188.

Zenk, W., and E. Morozov (2007), Decadal warming of the coldest Antarctic Bottom Water flow through the Vema Channel, *Geophysical Research Letters*, *34*(14), 1-5.

Zotikov, I. A., V. S. Zagorodnov, and J. V. Raikovsky (1980), Core drilling through the Ross Ice Shelf (Antarctica) confirmed basal freezing, *Science*, *207*(4438), 1463-1464.

Zwally, H. J., J. C. Comiso, C. L. Parkinson, D. J. Cavalieri, and P. Gloersen (2002), Variability of Antarctic sea ice 1979-1998, *Journal of Geophysical Research-Oceans*, *107*(C5), 1-19.